

POLITECNICO DI TORINO

Master of Science in Automotive Engineering

“IRON LOSS ESTIMATION UNDER PULSE WIDTH
MODULATION EXCITATION IN PERMANENT MAGNET
SYNCHRONOUS MOTORS”



Advisor:

Gianmario Pellegrino

Co-advisor:

Brian Sangeorzan

Candidate:

Filippo Bellone

Academic Year 2019/2020

© by Filippo Bellone, 2020
All rights reserved

Alla mia famiglia e Alessandra per il continuo supporto ed incoraggiamento.

*A Giulio e Marco per aver condiviso con me questa esperienza e a tutti
i miei amici per essere sempre stati presenti nonostante la distanza.*

ACKNOWLEDGMENTS

First of all, I am grateful to Dr. Arfakhshand Qazalbash and Dr. Subhra Paul for the continuous support provided in my research, for sharing their knowledge on a topic that was completely new to the author and for providing confrontation and advice throughout my time working at Oakland University and FCA.

I am also thankful to Dr. Nassar and Dr. Sangeorzan for welcoming me to Oakland University, for their help and for their guidance during my time in the United States.

ABSTRACT

As environmental concerns grow globally, the necessity to reduce polluting emissions is of key importance to the survivability of the automotive industry. The continuously rising number of vehicles that employ hybrid or fully electric powertrains leads to the need for more efficient electric machines.

The most commonly used type of electric motor in the vehicular application field is the permanent magnet synchronous motor, thanks to its high power-density and efficiency. When implemented in a vehicle, the electric machine is fed by a PWM supply, whose harmonic content increases the power loss of the motor.

The scope of this research is to improve the accuracy of the iron loss prediction in permanent magnet synchronous motors fed by PWM supply, employed in traction applications. The ability to estimate the loss quickly and correctly is of fundamental importance in the early stages of machine design, allowing proper optimization.

In this work, a new iron loss estimation method using finite element analysis software is introduced. First, an overview of iron loss in electrical machines is given, presenting its physical meaning and the modelling approaches present in the literature, based on the concept of loss separation.

The implementation procedure of the estimation method is explained and its performance is analyzed and compared to the standard estimation procedure applied in the industry. Last, the estimation method is validated on a second motor application to better understand its behavior and overall performance.

TABLE OF CONTENTS

ACKNOWLEDGMENTS	iv
ABSTRACT	v
LIST OF TABLES	x
LIST OF FIGURES	xii
NOMENCLATURE	xiv
CHAPTER ONE	
INTRODUCTION AND LITERATURE REVIEW	1
1.1. Introduction	1
1.2. Overview of Electrical Machine Losses	2
1.2.1. Mechanical Losses	3
1.2.2. Winding Losses	3
1.2.3. Iron Losses	4
1.3. Iron Loss Components and Separation Approaches	4
1.3.1. Hysteresis Losses	5
1.3.2. Eddy Current Losses	7
1.3.3. Excess Losses	7
1.4. Iron Loss Modelling	8
1.4.1. Constant Coefficients Model	8
1.4.2. Variable Coefficients Model	9
1.4.3. Effects of Pulse Width Modulation Supply and Fourier Analysis of Iron Loss	11
1.4.4. Rotational Loss	14
1.4.5. Saturation Loss	15
1.4.6. Influence of Temperature on Iron Loss	15
1.4.7. Influence of Machining on Iron Loss	16

TABLE OF CONTENTS - Continued

CHAPTER TWO	
METHODOLOGY	17
2.1. Scope of the Work	17
2.2. Analysis Setup	18
2.2.1. Lamination Material Hysteresis Loop Data	18
2.2.2. Interior Permanent Magnet Synchronous Motor Finite Element Analysis Model	18
2.2.3. Pulse Width Modulation Current Generation Model	20
2.2.4. Electric Motor Iron Loss Test Data	22
2.3. Iron Loss Model Development	23
2.3.1. Lamination Test Data Analysis	23
2.3.2. Constant Coefficients Models	24
2.3.3. Variable Coefficients Model	26
2.3.4. Performance Comparison	27
2.4. Finite Element Analysis Implementation	29
2.4.1. Pulse Width Modulation Currents Generation	29
2.4.2. Iron Loss Baseline Evaluation	30
2.4.3. Variable Coefficients Model Implementation	32
CHAPTER THREE	
IRON LOSS ESTIMATION	38
3.1. Iron Loss Test Data and Estimations	38
3.1.1. Iron Loss Test Data	38
3.1.2. Baseline Iron Loss Estimation	38
3.1.3. Variable Coefficients Model Iron Loss Estimation	40
3.2. Second Motor Analysis Setup	40

TABLE OF CONTENTS - Continued

3.2.1. Finite Element Analysis Model	43
3.2.2. Pulse Width Modulation Current Generation Model	44
3.2.3. Coreloss_user.data Input File and Variable Coefficients Evaluation	44
3.3. Iron Loss Test Data and Estimations on the Second Motor	47
3.3.1. Iron Loss Test Data of the Second Motor	47
3.3.2. Baseline Model Iron Loss Estimate on the Second Motor	47
3.3.3. Variable Coefficients Model Iron Loss Estimate on the Second Motor	48
CHAPTER FOUR	
ANALYSIS OF RESULTS AND DISCUSSION	52
4.1. Performance Analysis on the First Motor	52
4.1.1. Baseline Model Performance Analysis on the First Motor	52
4.1.2. Variable Coefficients Model Performance Analysis on the First Motor	52
4.1.3. Performance Comparison of the Models on the First Motor	55
4.1.4. Mean Absolute Prediction Error and Speed Range Subdivision Analysis on the First Motor	55
4.2. Performance Analysis on the Second Motor	56
4.2.1. Baseline Model Performance Analysis on the Second Motor	56
4.2.2. Variable Coefficients Model Performance Analysis on the Second Motor	59
4.2.3. Performance Comparison of the Models on the Second Motor	59
4.2.4. High Speed Mean Absolute Percentage Error and Absolute Loss Difference Analysis on the Second Motor	63
4.3. Discussion	64

TABLE OF CONTENTS - Continued

4.3.1. Magnetic Induction Analysis	64
4.3.2. Estimation Accuracy Comparison Between Motors	67
CHAPTER FIVE	
CONCLUSIONS AND FUTURE WORK	71
5.1. Conclusions	71
5.2. Future Work	72
APPENDICES	74
A. Data Tables	74
B. Copyright Permission Letters	79
REFERENCES	82

LIST OF TABLES

Table 2.1	Iron loss model coefficients	25
Table 2.2	Mean absolute percentage error of each model	27
Table 2.3	Variable coefficient analysis input parameters	36
Table 3.1	Iron loss test data	39
Table 3.2	Baseline model iron loss estimate	41
Table 3.3	Variable coefficients model iron loss estimate	42
Table 3.4	Variable coefficient analysis input file of the second IPMSM	45
Table 3.5	Iron loss test data of second IPMSM	49
Table 3.6	Baseline iron loss estimate on the second IPMSM	50
Table 3.7	VarKhKc iron loss estimate on the second IPMSM	51
Table 4.1	Percentage error of the baseline model estimation	53
Table 4.2	Percentage error of the VarKhKc model estimation	54
Table 4.3	Absolute percentage error difference between VarKhKc and baseline models	57
Table 4.4	MAPE comparison of baseline and VarKhKc models	58
Table 4.5	Percentage error of the baseline model estimation on the second IPMSM	60
Table 4.6	Percentage error of the VarKhKc model estimation on the second IPMSM	61
Table 4.7	Absolute percentage error difference between VarKhKc and baseline models on the second IPMSM	62
Table 4.8	MAPE and average iron loss estimate comparison of the two models above 7000 rpm on the second IPMSM	63

LIST OF TABLES -Continued

Table A.1	Values of K_h as function of peak magnetic induction	75
Table A.2	Values of K_c as function of frequency and peak magnetic induction	76
Table A.3	I_d values for PWM current generation	77
Table A.4	I_q values for PWM current generation	77
Table A.5	I_d values for PWM current generation of the second IPMSM	78
Table A.6	I_q values for PWM current generation of the second IPMSM	78

LIST OF FIGURES

Figure 1.1	Electrical machines total loss components	2
Figure 1.2	Modelled hysteresis loops including the effects of eddy current and excess losses	11
Figure 1.3	PWM voltage and resulting induction waveform	13
Figure 1.4	Dependence of r on induction in non-oriented SiFe laminations	14
Figure 2.1	Methodology of the research	17
Figure 2.2	Hysteresis loop at $f=400\text{Hz}$ and $\hat{B}=1.6\text{ T}$	19
Figure 2.3	Hysteresis loop at $f=1000\text{Hz}$ and $\hat{B}=1.6\text{ T}$	19
Figure 2.4	Ansys Maxwell™ model of the IPMSM	20
Figure 2.5	PWM currents generation circuit	21
Figure 2.6	IPMSM iron loss test data	22
Figure 2.7	Iron loss per unit mass as function of magnetic induction at different magnetization frequencies	24
Figure 2.8	MATLAB™ curve fitting app	25
Figure 2.9	Comparison of iron loss estimate of model 1, 2 and 3 at $f=50\text{ Hz}$	28
Figure 2.10	Comparison of iron loss estimate of model 1, 2 and 3 at $f=400\text{ Hz}$	28
Figure 2.11	Comparison of iron loss estimate of model 1, 2 and 3 at $f=2000\text{ Hz}$	29
Figure 2.12	PWM currents for $N_s=4000\text{ rpm}$ and 0.23 pu torque	31
Figure 2.13	PWM currents for $N_s=10000\text{ rpm}$ and 0.68 pu torque	31
Figure 2.14	Iron loss plot at $N_s=14000\text{ rpm}$ and 0.5 pu torque	32

LIST OF FIGURES -Continued

Figure 2.15	Coreloss_user.data input file structure	33
Figure 2.16	Solution setup settings	34
Figure 2.17	Iron loss simulation results output file	37
Figure 3.1	Ansys Maxwell™ 2D model of the second IPMSM	43
Figure 3.2	PWM current generation model of the second IPMSM	44
Figure 3.3	Iron loss per unit mass as function of magnetic induction at different magnetization frequencies of the lamination material of the second motor	46
Figure 4.1	Magnetic induction magnitude plot at 1600 rpm and 0.51 pu torque of the default simulation (a) and variable coefficients simulation (b)	65
Figure 4.2	Magnetic induction magnitude plot at 2400 rpm and 0.51 pu torque of the default simulation (a) and variable coefficients simulation (b)	66
Figure 4.3	Magnetic induction magnitude plot of the first motor at 6000 rpm and 1 pu torque	69
Figure 4.4	Magnetic induction magnitude plot of the second motor at 4600 rpm and 1 pu torque	69
Figure 4.5	Magnetic induction magnitude plot of the first motor at 14000 rpm and 0.5 pu torque	70
Figure 4.6	Magnetic induction magnitude plot of the second motor at 16000 rpm and 0.22 pu torque	70

NOMENCLATURE

PWM	Pulse width modulation
PMSM	Permanent magnet synchronous motor
FEA	Finite element analysis
P_b	Bearing power loss
μ_{fr}	Friction coefficient
F_b	Equivalent dynamic bearing load
D_b	Bearing bore diameter
ω	Angular frequency
CFD	Computational fluid dynamics
P_{cu}	Winding power loss
R_{ph}	Phase resistance
I	Current
RMS	Root mean square
DC	Direct current
P_{fe}	Iron loss per unit volume
P_{stat}	Static loss per unit volume
P_{dyn}	Dynamic loss per unit volume
P_h	Hysteresis loss per unit volume
P_c	Classical eddy current loss per unit volume
P_e	Excess loss per unit volume
f	Magnetizing frequency
B	Magnetic induction

NOMENCLATURE - Continued

H	Magnetic field strength
K_h	Hysteresis loss coefficient
α	Hysteresis loss power coefficient
k_m	Hysteresis loop loss coefficient
E	Electric field
t	Time
\hat{B}	Peak magnetic induction
d	Lamination thickness
ρ_e	Electrical resistivity
P_c^s	Eddy current loss per unit volume under sinusoidal excitation
K_c	Eddy current loss coefficient
G	Non-dimensional coefficient
V_0	Characteristic field
S	Lamination surface area
MO	Magnetic object
K_{SE}	Steinmetz iron loss coefficient
β	Steinmetz magnetic induction exponent
K_e	Excess loss coefficient
W_h	Hysteresis energy loss per unit volume
n	Harmonic order
B_n	Amplitude of the n-th harmonic of the induction waveform
ϕ_n	Phase shift of the n-th harmonic of the induction waveform

NOMENCLATURE - Continued

P_h^s	Hysteresis loss per unit volume under sinusoidal excitation
P_e^s	Excess loss per unit volume under sinusoidal excitation
F_c	Form factor coefficient
τ_i	Width of the i-th pulse of the PWM waveform
$P_{h,rot}$	Hysteresis loss considering the rotational flux component
$P_{h,alt}$	Hysteresis loss considering alternating flux only
$P_{fe,rot}$	Iron loss considering the rotational flux component
$P_{fe,alt}$	Iron loss considering alternating flux only
c	Short-axis-to-long-axis ratio of the flux vector ellipse
r	Rotational loss coefficient (1)
γ	Rotational loss coefficient (2)
$P_{c,sat}$	Eddy current loss including the effect of saturation
a_3	Higher order term multiplicative parameter
a_4	Higher order term exponent
FCA	Fiat Chrysler Automobiles
IPMSM	Interior permanent magnet synchronous motor
pu	Per unit
AC	Alternating current
N_s	Synchronous speed
p	Number of poles
T	Torque
L_d	D-axis inductance

NOMENCLATURE - Continued

L_q	Q-axis inductance
I_d	D-axis current
I_q	Q-axis current
ψ_m	Flux linkage of the permanent magnets
W_{fe}	Iron energy loss per unit volume
ρ	Volumetric density
MAPE	Mean absolute percentage error
A_i	Observed value
F_i	Forecast value

CHAPTER ONE

INTRODUCTION AND LITERATURE REVIEW

1.1 Introduction

Due to the growing environmental concerns regarding energy consumption, governments and industries have required the development of more efficient electrical machines in all application fields. More stringent regulations on greenhouse gas emissions have shifted the interest of the automotive industry and its customers towards electric powered vehicles, of which efficient electric motors are a key enabling technology. Electrical machines for traction application are required to have high torque and power densities, along with high efficiency, over a wide range of torque and speed, all at the lowest possible cost. Of the many electric machines available, permanent magnet synchronous motors (PMSM) have been adopted in many applications, and hence, PMSM play a key role in fulfilling the aforementioned properties [1][2].

An accurate estimation of the motor's power loss during the design phase is necessary to allow for proper optimization of its development and to achieve good performance. The main focus of this research will be on iron losses, one of the three components that contribute to the total power loss. These losses are generated in the ferromagnetic core of the machine by time-varying magnetic fields. Electric motors used for traction in vehicles are supplied by a 3-phase inverter controlled by a pulse width modulation (PWM) algorithm; the PWM supply generates a non-sinusoidal signal that is polluted with harmonics (i.e. higher frequencies). The presence of harmonics in the current supply increases the total iron losses in the machine with respect to an ideal sinusoidal excitation and must be correctly modelled at all

operating conditions. This type of simulation is not an easy task due to expensive computations, but an indispensable one [3]-[8]. The objective of this research work is to create an analytical model, easily implementable in 2D FEA post-processing, able to take into consideration the effects of PWM supply on iron losses in permanent magnet synchronous machines.

1.2 Overview of Electrical Machine Losses

The correct estimation of total losses in electrical machines is of crucial importance to the evaluation of their efficiency, which is one of the main targets during design optimization process. The power losses can be divided into three main categories, as shown in Fig. 1.1.

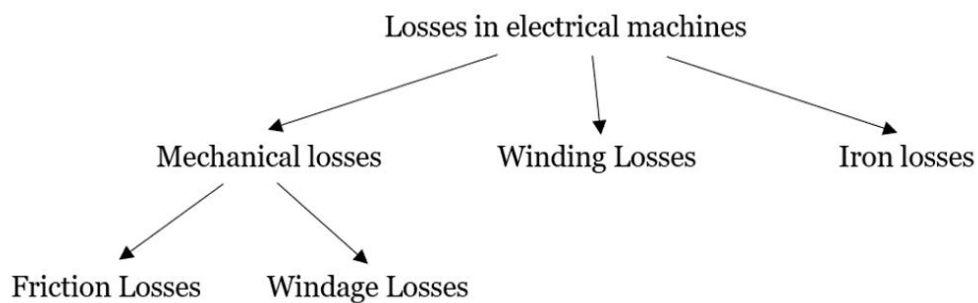


Figure 1.1. Electrical machines total loss components

They include mechanical, winding and iron losses: their respective influence on total power losses varies depending on many factors, such as machine type and size [9]. A quick overview of the origin of each loss is briefly provided in this section.

1.2.1 Mechanical Losses

Mechanical losses include frictional losses (i.e. related to the bearings) and windage losses (i.e. related to gas friction). Power loss in bearings can be estimated using well-defined formulas provided by the manufacturer. According to SKF (well-known European bearing supplier) power loss in bearings is calculated as follows:

$$P_b = 0.5\mu_{fr}F_bD_b\omega \quad (1.1)$$

where μ_{fr} is the friction coefficient of the bearing, F_b is the equivalent dynamic bearing load, D_b is the bearing bore diameter and ω is the angular frequency [9][10]. Power loss increases proportionally to the rotational speed.

Windage losses, on the other hand, are generated by the gas friction between the rotating mass of the rotor and the gas in the air gap. These losses are dependent on the geometry of the machine, which makes it difficult to obtain an analytical equation for their evaluation and thus they are usually computed through CFD simulations.

1.2.2 Winding Losses

Winding losses (also referred to as copper or ohmic losses) are generated by the current flowing through the conductors in the stator slots in form of Joule heating and in a 3-phase machine are obtained using Eq. (1.2)

$$P_{cu} = 3R_{ph}I^2 \quad (1.2)$$

where R_{ph} is the phase resistance and I is the RMS value of the phase current [9]. In principle, winding losses seem simple to evaluate by applying Ohm's law but there are two main factors affecting its accuracy that must be taken into account: the temperature dependence of the wires' resistivity and the skin effect. The increasing resistivity of the copper wires with temperature will generate higher copper loss and an accurate thermal model is necessary to correctly predict its behavior. Moreover, the

skin effect, due to the alternating currents in the conductors, generates eddy currents through electromagnetic interaction: these eddy currents tend to oppose the current flow and are not symmetrically distributed in the cross-section of the wires along the radial direction, ultimately altering the current density distribution in the conductor [4]. This will result in a higher current flowing on the outer region (i.e. the skin) of the conductor, increasing total copper loss due to its quadratic dependence on current; this effect is especially prominent at higher frequency.

1.2.3 Iron Losses

Iron or core losses are generated by the alternating magnetic field in the ferromagnetic material of the stator and the rotor. From the physical point of view, these losses are due magnetic domain wall movement during the change in magnetization of the material [11][12]. The movement of domain walls generates eddy currents which in turn generate Joule heating. Iron losses are usually divided in static and dynamic losses, being independent or dependent on the magnetization frequency, respectively.

1.3 Iron Loss Components and Separation Approaches

Iron losses are a fundamental component of total loss in electrical machines used for traction applications and constitute the predominant losses in the machine during field weakening operation [11]. Iron losses are based on the same physical phenomenon: during the change in magnetization, the movement of domain walls generates microscopic and macroscopic eddy currents which in result dissipate energy in form of Joule heating. This phenomenon happens even at DC magnetization. During DC magnetization, the external field changes slowly, but the movement of the domain walls is discrete in time and the alignment of the magnetic moment of the

single domains can be very rapid. This phenomenon causes loss, which is known as hysteresis losses and it happens also at very low frequency [11][12].

A common approach to analyze iron losses is by separating the losses into different groups: static and dynamic (as shown in Eq. (1.3)). The static loss, also known as hysteresis loss, dissipates the same energy per cycle independent of the magnetization frequency while the dynamic loss component is frequency dependent.

$$P_{fe} = P_{stat} + P_{dyn} \quad (1.3)$$

This separation procedure is an engineering empirical approach that tries to evaluate separately the dependencies of total loss on frequency and induction, without explaining the physical phenomena directly, and then, allows engineers to quickly estimate losses during the design phase.

The dynamic term was modeled using only classical eddy current, and later expanded by Bertotti [13][14] to include excess loss (known as anomalous loss) as well. Accordingly, total losses can be expressed by three terms as provided in Eq.

(1.4)

$$P_{fe} = P_h + P_c + P_e \quad (1.4)$$

where P_h is the hysteresis loss, P_c is the classical eddy current loss and P_e is the excess loss term.

1.3.1 Hysteresis Losses

Hysteresis loss per cycle is related to the area of the quasi-static hysteresis loop and the energy loss is considered to be independent of the frequency [3][4][8]: total power loss per unit volume is obtained by multiplying the loss per cycle with the magnetizing frequency [7]:

$$P_h = f \oint H dB \quad (1.5)$$

where f is the magnetizing frequency, H is the magnetic field strength and B is the magnetic induction (also referred to as magnetic flux density). It is often assumed that in the absence of minor hysteresis loops this loss is directly proportional to f regardless of the shape of the wave [3]. Therefore, it can be evaluated experimentally with quasi-static measurements on an Epstein frame under sinusoidal excitation [15]. In analytical models hysteresis loss is calculated using Steinmetz's equation:

$$P_h = K_h f \hat{B}^\alpha \quad (1.6)$$

where \hat{B} is the peak magnetic induction, K_h and α are experimental coefficients.

There are models, such as the ones developed in [6][15][16], in which α is considered a constant (equal to 2) and models in which the parameter is obtained, along with K_h , by fitting Eq. (1.6) on measured loss data [17].

The assumption of constant loss per cycle holds only in the absence of hysteresis minor loops, which are generated by reversals in the induction waveform ([7][15][18]), caused by harmonics in the excitation due to PWM supply[3][4][6][8]. In the presence of minor loops, an algorithm must be employed to detect them and models including a corrector factor must be developed, such as the one expressed in Eq. (1.7).

$$P_h = K_h f \hat{B}^\alpha \left[1 + \frac{k_m}{\hat{B}} \sum_{i=1}^j \Delta B_i \right] \quad (1.7)$$

k_m is a material dependent parameter (typically between 0.6 and 0.7), j is the number of minor loops and ΔB_i is the amplitude of the i -th reversal in the induction waveform [6][18][19]. Equation (1.7) can be employed for the analytical calculation of the additional loss related to the area of the minor loops.

1.3.2 Eddy Current Losses

Classical eddy currents are described by solving the so-called Maxwell-Faraday equation for a given geometry, assuming uniform penetration of the magnetic field inside the material [20]

$$\nabla \times E = -\frac{dB}{dt} \quad (1.8)$$

where E is the electric field. For a thin lamination Eq. (1.9) is obtained [3]

$$P_c = \frac{d^2}{12\rho_e} \left(\frac{dB(t)}{dt} \right)^2 \quad (1.9)$$

where d is the lamination thickness and ρ_e is the material electrical resistivity. For sinusoidal excitation Eq. (1.9) can be simplified to [4][15][20]

$$P_c^s = \frac{\pi^2 d^2}{6\rho_e} f^2 \hat{B}^2 \quad (1.10)$$

where the superscript s is used to indicate that the excitation is sinusoidal. In analytical models a generic expression is used

$$P_c = K_c (f\hat{B})^2 \quad (1.11)$$

where K_c is the eddy current loss coefficient, an experimental coefficient to be evaluated through fitting of the equation on measured loss data.

1.3.3 Excess Losses

Early research by Pry and Bean [21] showed that hysteresis and classical eddy current losses were not sufficient to describe the measured loss and initially an anomalous loss coefficient was added to the eddy current loss term to consider for this discrepancy. This “anomalous” loss component was extensively researched by Bertotti, who explained its physical meaning in [14], based on the concept of magnetic object: “the basic physical mechanism governing excess losses in soft materials is identified with the competition between the external magnetic field,

applied uniformly in the sample, and highly inhomogeneous local counterfields due to eddy currents and microstructural interactions”. The expression to evaluate excess loss under sinusoidal excitation is reported in [3][7], which for a thin lamination is calculated using the following equation

$$P_c^s = 8.67 \sqrt{\frac{GV_0 S}{\rho_e}} (f \hat{B})^{1.5} \quad (1.12)$$

where $G \approx 0.1356$ is a non-dimensional coefficient and V_0 , a parameter dependent on the material microstructure, is the characteristic field controlling the number of simultaneously active MOs brought about by an external field [7][13][14][20]. S is the surface area of the lamination. This equation can be generalized to

$$P_e = K_e (f \hat{B})^{1.5} \quad (1.13)$$

In analytical core loss models, K_e is the excess loss coefficient and has to be obtained by fitting Eq. (1.13) on measured loss data.

1.4 Iron Loss Modelling

1.4.1 Constant Coefficients Models

The simplest loss models employ constant coefficients, independent of frequency and induction. The first model of iron loss was proposed by Steinmetz based on the following equation

$$P_{fe} = K_{SE} f^\alpha \hat{B}^\beta \quad (1.14)$$

where the three coefficients α , β and K_{SE} are evaluated by fitting the equation on measured loss data. This model assumed sinusoidal flux density, and thus, many revisions of the equation were proposed in order to improve it, including the Modified Steinmetz Equation and the Generalized Steinmetz Equation, among others. These models require little prior knowledge of the material but the results are not

satisfactory. The first two-term model was proposed by Jordan [22], and included a static (or hysteresis) term and a dynamic (or eddy current) term.

$$P_{fe} = P_{stat} + P_{dyn} \quad (1.15)$$

Jordan assumed the static portion of the losses to be proportional to the area of the quasi-static hysteresis loop and the dynamic portion to be made up of classical eddy current loss exclusively, according to (1.9). The inaccuracy of this model for *SiFe* alloys ultimately led to the addition of a third term by Bertotti, which resulted in the most popular iron loss model in use nowadays:

$$P_{fe} = K_h f B^2 + K_c (fB)^2 + K_e (fB)^{1.5} \quad (1.16)$$

To obtain the three coefficients of this model, loss measurements are carried out on a single lamination using an Epstein frame under sinusoidal excitation; it is therefore not suitable to predict the loss behavior in presence of harmonics, skin effect and minor hysteresis loops.

1.4.2 Variable Coefficients Models

The fitting procedure of constant coefficient models uses measured loss data across many induction values, usually up to $1.7 \div 2T$, and a broad frequency range; this simplified approach can be improved by considering dependence on induction of the coefficients. By dividing the induction spectrum in two or more sections and applying the same fitting procedure on each data set we are able to obtain more accurate results.

This concept is applied to the evaluation of hysteresis loss in [6], where two intervals of the magnetic flux density are defined based on the position of the “knee” in the material’s magnetization curve. Assuming the knee to be at $B=1T$, hysteresis

losses per cycle per unit volume are evaluated as given in Eq. (1.17). This new expression improves the accuracy of the estimation of the model.

$$W_h = \begin{cases} K_{h1}B^{\alpha_1}, & x < 1T \\ K_{h2}B^{\alpha_2}, & x \geq 1T \end{cases} \quad (1.17)$$

A much more complex model is proposed in [23], where the hysteresis loss coefficient is considered to be a function of f and B while the eddy current loss and excess loss coefficients are regarded as variable with induction only. The curve fitting of K_e and K_c was carried out with third-order polynomials resulting in

$$K_e = K_{e0} + K_{e1}B + K_{e2}B^2 + K_{e3}B^3 \quad (1.18)$$

for the excess loss coefficient and likewise for the eddy current loss coefficient. The evaluation of the hysteresis loss coefficient and hysteresis loss power coefficient is performed by dividing the induction in three ranges: $0 \div 0.7$, $0.7 \div 1.4$ and $1.4 \div 2T$. The values of α and K_h are then evaluated through linear regression at 5 frequency values for each induction range ($f=25, 60, 120, 300$ and 400Hz). This model proved to be very accurate, although it requires a lot of measurements and the fitting procedure is quite articulated.

The dependency of the hysteresis loop area, and thus, the hysteresis loss, on the magnetizing frequency was already investigated in 1994 by Jiles [20], who modelled the influence of the dynamic loss components on the shape of the hysteresis loop at increasing frequency. The experimental results showed an increase of coercivity of the material increasing with frequency while the remanence is independent and remains constant. The loops model, shown in Fig. 1.2, is in good agreement with the measured data; the analytical expression of the model is not reported for sake of simplicity as it is not beneficial to the engineering approach proposed for this research work.

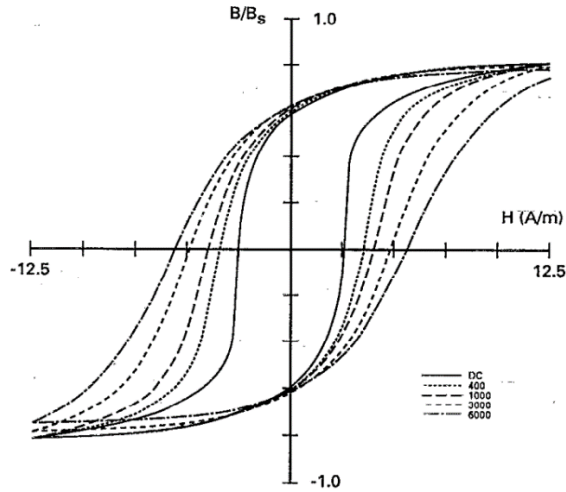


Figure 1.2. Modelled hysteresis loops including the effects of eddy current and excess losses

From “Frequency Dependence of Hysteresis Curves in Conducting Magnetic Materials”, by D. C. Jiles, 1994, *Journal of Applied Physics*, 76. Copyright 1994 by the American Institute of Physics. Reprinted with permission.

1.4.3 Effects of Pulse Width Modulation Supply and Fourier Analysis of Iron Loss

Although the desired shape of the induction waveform in the core of the machine is sinusoidal, due to factors like iron saturation and PWM excitation, practical magnetic cores are subject to non-sinusoidal flux, especially in regions such as the tooth tip. This causes an increase of the losses with respect to sinusoidal regime: the prediction of iron loss under arbitrary flux waveform becomes then of fundamental importance [3]-[8].

An approach to compute the loss due to an arbitrary waveform is to express the induction and its derivative as a Fourier expansion

$$B(t) = \sum_n B_n \sin(2n\pi ft + \phi_n) \quad (n = \text{odd}, \phi_1 = 0) \quad (1.19)$$

$$\dot{B}(t) = \sum_n 2n\pi f B_n \cos(2n\pi f t + \phi_n) \quad (n = \text{odd}, \phi_1 = 0) \quad (1.20)$$

where n is the harmonic order, B_n and ϕ_n are the amplitude and phase shift of the n -th harmonic component. This methodology, employed by Fiorillo and Novikov [7], requires to measure hysteresis loss and total loss under sinusoidal regime at an arbitrary frequency f_0 and the knowledge of the harmonic content in order to predict with good accuracy the iron loss due to an arbitrary flux waveform. The loss under sinusoidal regime for a thin lamination can be calculated analytically using Eqs. (1.5, 1.10 and 1.12), obtaining

$$P_{fe}^s = P_h^s + P_c^s + P_e^s = P_h(f_0) + \frac{\pi^2 d^2}{6\rho_e} (f_0 \hat{B})^2 + 8.67 \sqrt{\frac{GV_0 S}{\rho_e}} (f_0 \hat{B})^{1.5} \quad (1.21)$$

By comparing the measured loss to Eq. (1.21), it is possible to obtain the value of GV_0 , which can then be used to evaluate the loss under an arbitrary non-sinusoidal waveform:

$$P_h(f) = P_h^s(f_0) \cdot \frac{f}{f_0} \quad (1.22)$$

$$P_c(f) = \frac{\pi^2 d^2}{6\rho_e} f^2 \cdot \sum_n n^2 B_n^2 \quad (1.23)$$

$$P_e(f) = \sqrt{\frac{GV_0 S}{\rho_e}} f \int_0^T \left| \sum_n 2n\pi f B_n \cos(2n\pi f t + \phi_n) \right|^{\frac{3}{2}} dt \quad (n = \text{odd}, \phi_1 = 0) \quad (1.24)$$

As the model relies on the hypothesis of independence of the hysteresis loop on the waveform, it is only applicable in the absence of minor hysteresis loop.

A simplification of this method, aimed at reducing the amount of prior knowledge required, is introduced in [8], where the iron loss under non-sinusoidal

waveform is calculated as a second order polynomial of a newly introduced form factor coefficient F_c , starting from the measured loss for sinusoidal excitation.

$$P_{fe} = P_h^s + P_c^s \cdot F_c^2 + P_e^s \cdot F_c \quad (1.25)$$

In the special case of PWM excitation, the form factor coefficient is evaluated as

$$F_c = \frac{2}{\pi \sqrt{f \sum_1^n \tau_i}} \quad (1.26)$$

where n is the number of pulses per half period and τ_i is the width of the i -th pulse, as shown in Fig. 1.3.

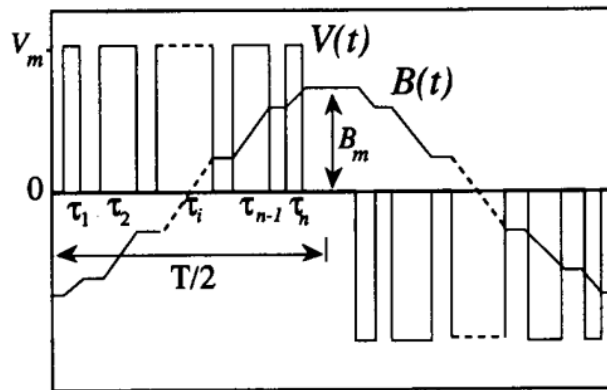


Figure 1.3. PWM voltage and resulting induction waveform

From “A General Formula for Prediction of Iron Losses Under Nonsinusoidal Voltage Waveform”, by M. Amar and R. Kaczmarek, 1995, IEEE Transaction on Magnetics, Vol. 31, No. 5. Copyright 1995 by the IEEE. Reprinted with permission.

This simplified approach yielded similar results to the previous model but, like its predecessor, it cannot predict the loss generated by the flux reversal in the induction waveform that happen when the harmonic content is high.

1.4.4 Rotational Loss

Another reason for the discrepancy between test data from Epstein frame measurements and FEA simulation results is the rotational flux component in the core of rotating machines, especially at the roots of the teeth, the back section of the slots and the front parts of teeth [24].

The equation proposed in [25] to account for the hysteresis loss increase in case of elliptic flux is

$$P_{h,rot} = [1 + c(r - 1)] \cdot P_{h,alt} = [1 + c(r - 1)]K_h f \hat{B}^2 \quad (1.27)$$

where c is the ratio of minor to major axis of the ellipse and r is an induction dependent parameter, as shown in Fig. 1.4. The subscript *rot* indicates the loss including the flux's rotational component while the subscript *alt* is used when only the alternating component of the flux is considered.

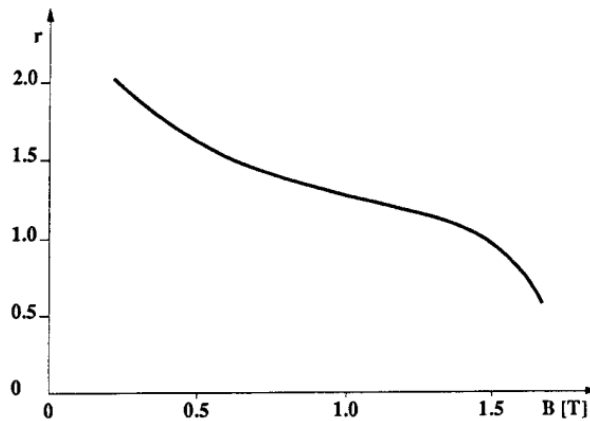


Figure 1.4. Dependence of r on induction in nonoriented SiFe laminations

From “An Improved Estimation of Iron Losses in Rotating Electrical Machines”, by G. Bertotti, A. Boglietti, M. Chiampi, D. Chiarabaglio, F. Fiorillo and M. Lazzari, 1991, IEEE Transactions on Magnetics, Vol. 27, No. 6. Copyright 1991 by the IEEE. Reprinted with permission.

In [24] a similar equation is proposed, in which the rotational loss coefficient is multiplied to both hysteresis and eddy current components

$$P_{fe,rot} = P_{fe,alt} \cdot (1 + \gamma c) \quad (1.28)$$

where c is again the minor-to-major axis ratio and γ is a parameter dependent on the lamination material and the induction level.

1.4.5 Saturation Loss

The Bertotti model tends to underestimate losses at high magnetic flux densities and high frequency by failing to account for the saturation of some regions of the core, such as the tooth tip. To compensate for this a higher order term is often added [15][26]:

$$P_{c,sat} = (1 + a_3 \hat{B}^{a_4}) \cdot P_c = K_c (1 + a_3 \hat{B}^{a_4}) f^2 \hat{B}^2 \quad (1.29)$$

In Eq. (1.29) two coefficients are introduced, a_3 and a_4 , to be determined based on the nonlinear material behavior at high frequency and induction. The exponent a_4 is dependent on the lamination thickness and typically assumes values between 2 and 6. Results in [26] show that consideration of flux harmonics helps to improve the accuracy of the results but it's not sufficient by itself: it's fundamental to consider also material saturation and the rotational loss component to further reduce the gap between FEA estimations and the measured loss.

1.4.6 Influence of Temperature on Iron Loss

All of the aforementioned models don't have an explicit dependence of loss on temperature. The research in [27] shows that the measured loss decreases moving from 69°C to 100°C. Although the variation of model coefficients with temperature, along with frequency and induction, should be taken into consideration if the goal is to achieve the highest level of accuracy. It should be noted that the temperature

dependence of iron loss will not be regarded in my research, being unable to perform the necessary measurements to obtain the correlation, and all the simulations will be performed using the materials properties at 100°C.

1.4.7 Influence of Machining on Iron Loss

It is well known that the measured loss of a machine core differs quite significantly from the estimates based on analytical models; whose parameters are usually obtained by fitting a set of equations on loss data measured on a single lamination of material. The production process together with the assembly process of machine cores lead to a deterioration of the magnetic properties of the material. The residual mechanical and thermal stresses generated by machining operations (such as punching and cutting) and by assembly operations (such as stacking and welding) reduce the permeability of the core, increasing the iron loss. An annealing process can be applied to relief some of the accumulated stress and partially restore the magnetic properties [9]. In addition to the induced stresses, damage to the insulating layer between laminations can be caused by these processes which will increase the eddy current loss in the electric machine.

CHAPTER TWO

METHODOLOGY

2.1 Scope of the Work

The scope of this research work is to develop an accurate iron loss estimation method for interior permanent magnet synchronous motors (IPMSM), easily implementable in FEA post-processing in Ansys Maxwell™. Currently, iron loss estimations calculated using FEA software require correction factors in order to be correlated to the test results; the correction factors can be as high as 2 or 3 for specific torque and speed points.

The developed method aims at reducing the discrepancy between simulation results and test data, in order to provide more reliable data that can be used in the early stages of the machine development process to optimize its design and reach performance and efficiency targets. A schematic of the methodology followed is presented in Figure 2.1; the starting point of the research are two set of experimental data and two Ansys Maxwell™ models, provided by suppliers or Fiat Chrysler Automobiles (FCA) directly.

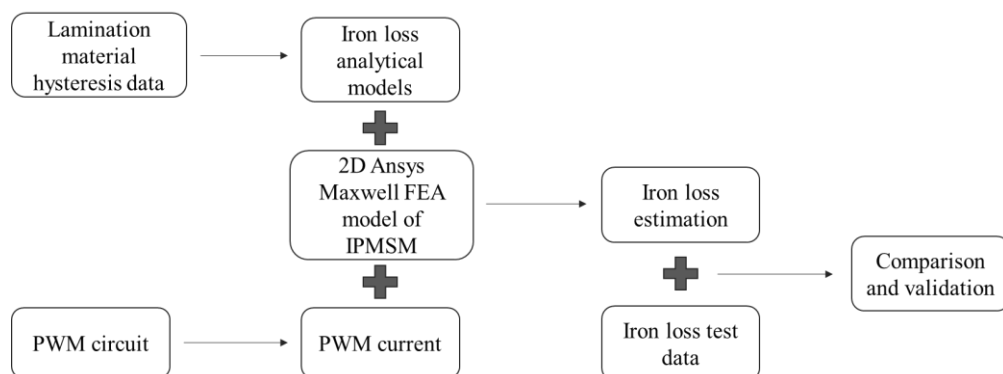


Figure 2.1. Methodology of the research

2.2 Analysis Setup

2.2.1 Lamination Material Hysteresis Loop Data

The test data, provided by the steel manufacturer, includes the measured magnetic induction in the lamination for varying magnetic field strength, at different magnetization frequencies f and peak magnetic inductions \hat{B} . The magnetization frequencies provided in the test results are 50, 100, 400, 1000 and 2000 Hz. For each frequency, the peak magnetic induction is increased in increments of 0.1 T, starting at $\hat{B}=0.1$ T all the way up to $\hat{B}=1.9$ T at $f_m=50$ Hz, 1.8 T at 100 Hz, 1.6 T at 400 and 1000 Hz and finally up to 1.2 T at 2000 Hz. The highest achievable peak magnetic induction is lower at higher frequency due to the onset of saturation. For each of the $f - \hat{B}$ combinations a hysteresis loop can be plotted, such as the ones reported in Figures 2.2 and 2.3. Given the same peak induction, hysteresis loops broaden with increasing frequency.

2.2.2 Interior Permanent Magnet Synchronous Motor Finite Element Analysis Model

A 2D FEA model of the IPMSM was developed in Ansys Maxwell™ to be used for the iron loss simulations. The material properties for the copper wires, the magnets and the electrical steel are imported for the operating temperature of 100 °C.

Taking advantage of the symmetry of the e-motor, by using Neumann and Dirichlet boundary conditions, only one eighth of the machine had to be modelled, as shown in Figure 2.4. This procedure allows to reduce computational times during the iron loss simulations. The electric motor under analysis is a 48 slot, 8 pole IPMSM with buried v-shaped magnets; it is fed by a 3-phase PWM inverter and operates at a nominal DC voltage of 350 V. The base speed is 6000 rpm and the maximum rotational speed achievable is 14000 rpm; torque and power rating cannot be disclosed and will be expressed in normalized terms as per unit (pu) of the maximum value.

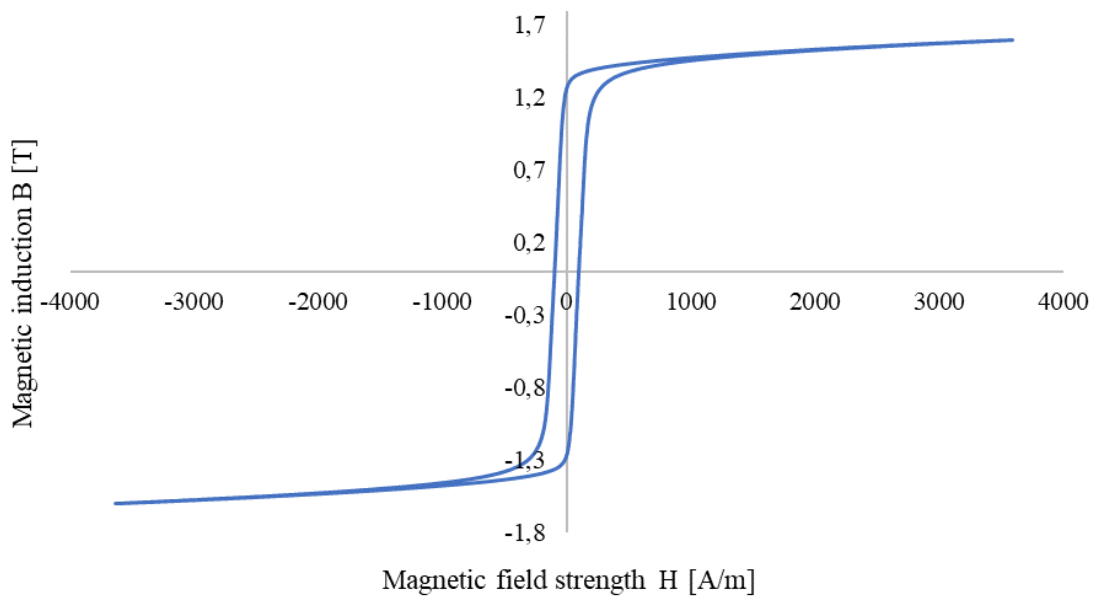


Figure 2.2. Hysteresis loop at $f=400\text{Hz}$ and $\hat{B}=1.6\text{ T}$

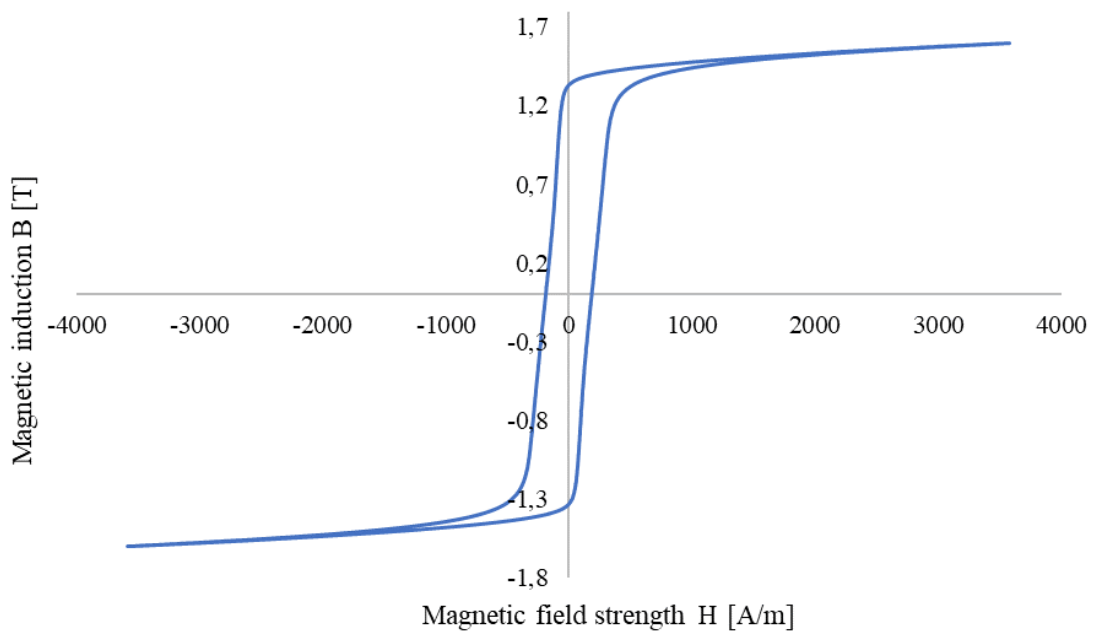


Figure 2.3. Hysteresis loop at $f=1000\text{Hz}$ and $\hat{B}=1.6\text{ T}$

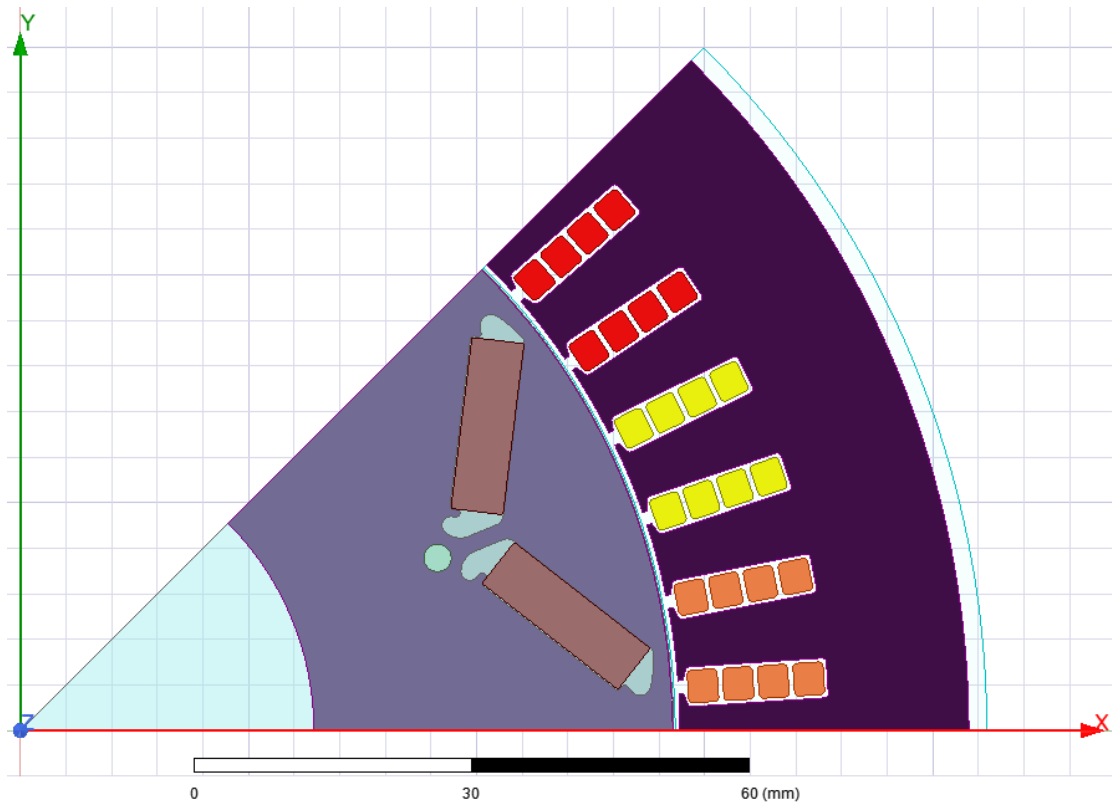


Figure 2.4. Ansys Maxwell™ model of the IPMSM

The permanent magnets are made of neodymium-iron-boron ($Ne_2Fe_{14}B$) whereas the electrical steel is a non-oriented $FeSi$ alloy, having 0.27 mm thick laminations. The motor has a skew rotor divided in three sections: the nominal one is in the middle and two sections, shifted respectively of +2.5 deg and -2.5 deg, are to each side. In a 2D simulation environment this is accounted for by running three iron loss calculation, shifting the initial position of the rotor, and averaging the results. A more complicated 3D simulation would only be marginally more accurate in this regard and the additional computational effort makes it an unfeasible option.

2.2.3 Pulse Width Modulation Currents Generation Model

To provide the correct PWM current input to the motor in the iron loss simulation environment, a model of the power electronics circuit must be used. The

Anslys model, developed by FCA and shown in Fig. 2.5, includes the 3-phase inverter, the equivalent circuit model of the electric motor and the PWM controller.

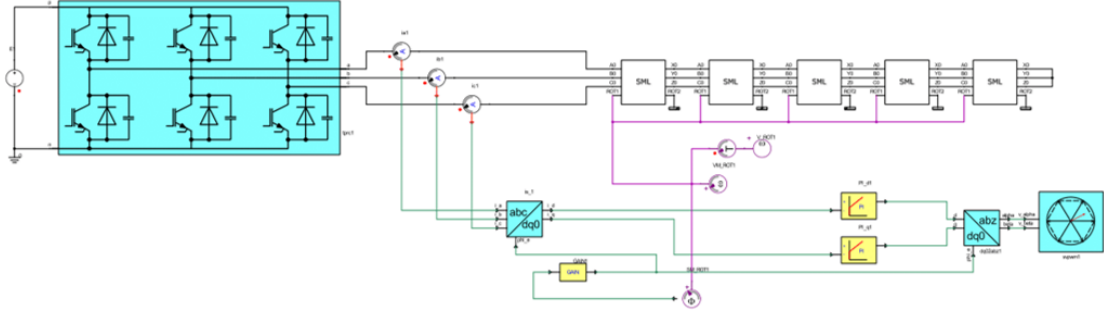


Figure 2.5. PWM currents generation circuit

In traction applications, an inverter is needed to convert the DC current output of the battery to a 3-phase AC current that can be fed to the motor. The operation of the inverter switches is controlled by the PWM algorithm, this is done to manipulate the frequency and amplitude of the output PWM current, which directly influence the operating point, i.e. rotational speed and torque, of the electric motor, according to Equations (2.1) and (2.2):

$$N_s = 120 \cdot \frac{f}{p} \quad (2.1)$$

where N_s is the rotational speed of the motor in rpm, i.e. the synchronous speed, f is the frequency of the current and p is the number of poles of the motor,

$$T = \frac{3p}{4} (\psi_m I_q + (L_d - L_q) I_d I_q) \quad (2.2)$$

where T is the output torque of the motor, ψ_m is the flux linkage of the permanent magnets, L_d and L_q are the d - and q -axis inductances of the PMSM and I_d and I_q are

the d - and q -axis currents. The inputs required by the model are the target speed, as well as the values of I_d and I_q .

2.2.4 Electric Motor Iron Loss Test Data

Although the research work takes place in a simulation environment, all the models were developed based on an already existing electric motor. The IPMSM was tested on a dynamometer, by FCA, to evaluate its iron loss component under different operating conditions; tests were performed for both no-load and load conditions, at 100°C. At on-load condition, the e-motor was tested with constant torque intervals from zero up to the maximum torque and speed intervals of 1000 rpm, from 1000 up to the maximum rotational speed of 14000 rpm. Iron loss in the motor were separated by subtracting the mechanical loss component and the conduction loss in the copper wires from the total loss measured on the machine; the accuracy of the result is estimated by FCA to be $\pm 5\%$. The obtained results are plotted in Fig.2.6.

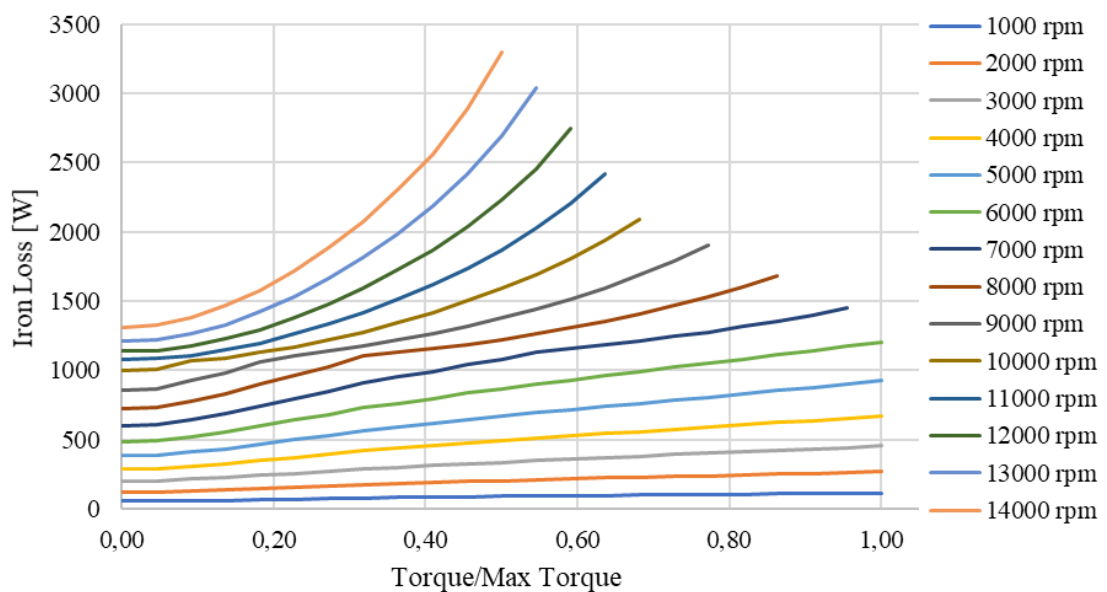


Figure 2.6. IPMSM iron loss test data

This data is later compared to the FEA estimations and used for validation of the developed estimation method.

2.3 Iron Loss Model Development

In this section, the provided hysteresis loop data is used to determine the dependency of the lamination material iron loss on magnetizing frequency and magnetic induction. The coefficients of different analytical iron loss equations are evaluated starting from the obtained loss data; these models are then used to estimate the lamination iron loss and their prediction accuracy is compared to determine the most suitable one, that will later be implemented in Ansys Maxwell™ for the iron loss estimation of the IPMSM under pulse width modulation excitation.

2.3.1 Lamination Test Data Analysis

The starting point for the development of the iron loss model is the hysteresis loop data of the lamination material used in the traction motor. Each loop area was numerically integrated using the *trapz* function in MATLAB™ to obtain the energy loss per unit volume as function of f and \hat{B} ; the results were then multiplied by the magnetization frequency to obtain the power loss per unit volume:

$$W_{fe} = \oint HdB \quad (2.3)$$

$$P_{fe} = f \cdot \oint HdB \quad (2.4)$$

Equation (2.4), although similar to Eq. (1.5), is actually representative of the total iron loss and not only of the hysteresis component. This is due to the fact that the integration is not carried out on the quasi-static hysteresis loop, but on the hysteresis loop measured at specific f values and therefore it includes the effects of the dynamic iron loss component as well. The evaluated values of $P_{fe}(f, \hat{B})$ were then multiplied

by the density of the steel, $\rho=7600 \text{ kg/m}^3$, to obtain the iron loss per unit mass; its dependency on \hat{B} at different frequencies is plotted in Figure 2.7.

These loss curves are then used for evaluating the coefficient of the various analytical equations, explained in the next sections, and to define the lamination material properties in the simulation environment.

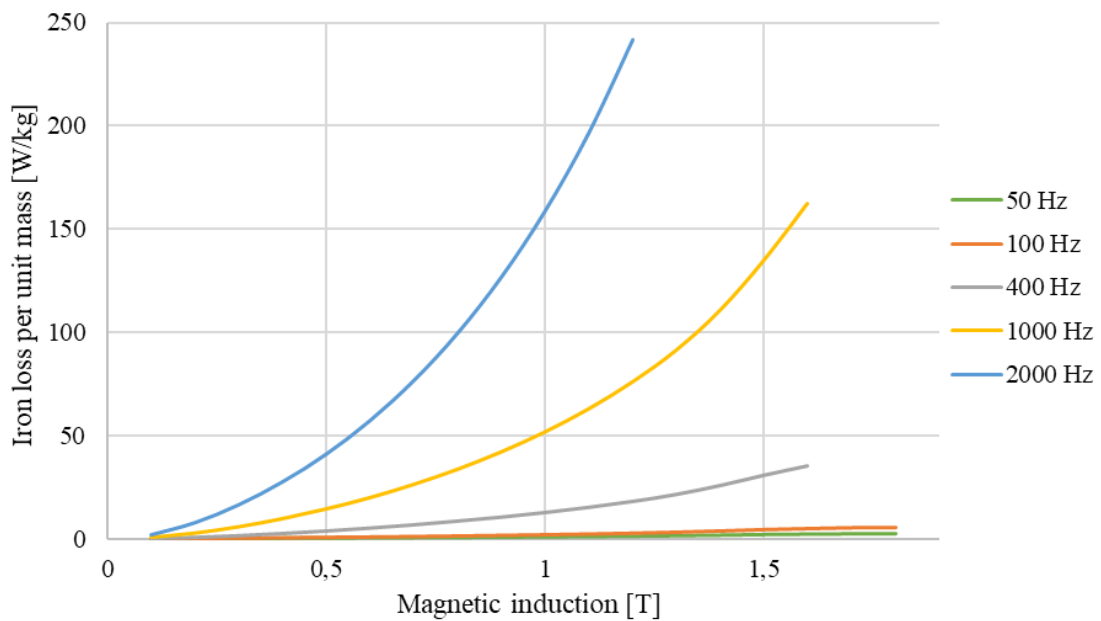


Figure 2.7. Iron loss per unit mass as function of magnetic induction at different magnetization frequencies

2.3.2 Constant Coefficients Models

The first analytical iron loss equation analyzed is a simple two-term constant coefficient model; this, as explained later, is also the model used by Ansys Maxwell™ for the estimation of iron loss on this particular lamination material.

1) Two-term

$$P_{fe} = K_h f \hat{B}^2 + K_c f^2 \hat{B}^2$$

Additionally, a three-term constant coefficient model, including a higher order term to better represent the loss behavior at high magnetic induction, was also analyzed.

$$2) \text{ Three-term with saturation} \quad P_{fe} = K_h f \hat{B}^2 + K_c f^2 \hat{B}^2 \cdot (1 + a_3 \hat{B}^{a_4})$$

After importing the loss curves into the MATLAB™ *curve fitting* app, as shown in Fig. 2.8, and specifying the custom equation representing the iron loss in function of the two variables f and \hat{B} , the model coefficients were obtained through a non-linear least squares method. The coefficients of each analytical model are reported in Table 2.1:

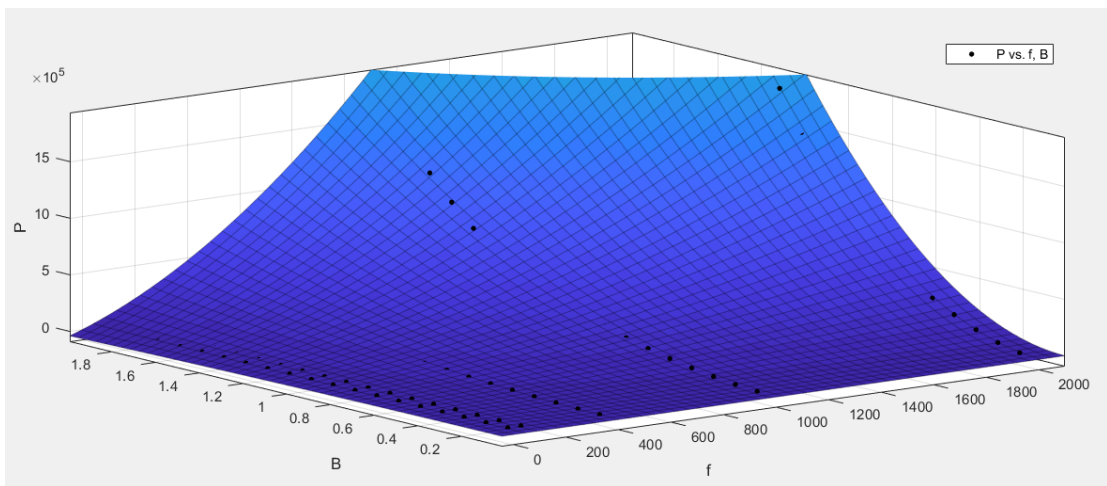


Figure 2.8. MATLAB™ curve fitting app

Table 2.1. Iron loss model coefficients

Model	K_h	K_c	a_3	a_4
1	220.4	0.2021	-	-
2	152.8	0.2213	0.03407	5.687

2.3.3 Variable Coefficients Model

The third model that was analyzed is a variable coefficient model based on the same equation of model 1:

$$3) \text{ Two-term variable coefficients} \quad P_{fe} = K_h(\hat{B})f\hat{B}^2 + K_c(f, \hat{B})f^2\hat{B}^2$$

In this particular analytical model K_h is no longer constant, but dependent on the peak magnetic induction, whereas K_c is now variable with both frequency and peak magnetic induction. The procedure followed to obtain the coefficients of the model is more complex than the constant coefficient models and it's the following: the power loss data is divided by the frequency to obtain the energy loss per unit volume W_{fe} , this is then plotted versus f for each level of peak magnetic induction.

$$W_{fe} = \frac{P_{fe}}{f} = K_h(\hat{B})\hat{B}^2 + K_c(f, \hat{B})f\hat{B}^2 \quad (2.5)$$

The curve is extrapolated to obtain the y-axis intercept, representing the energy loss at $f=0$ Hz (i.e. the static component of the loss); this value is used for the evaluation of $K_h(\hat{B})$. After subtracting the hysteresis energy loss component from W_{fe} , we are able to evaluate K_c for each combination of frequency and peak magnetic induction. The coefficient evaluation procedure was carried out in Ansys Maxwell™, using a Python script automated in the *Extraction of Core Loss Coefficients* toolkit; the values of $K_h(\hat{B})$ and $K_c(f, \hat{B})$, reported in the Appendix A, are exported in a .txt file that will later be used as input to the IPMSM iron loss calculation using the variable coefficient model.

2.3.4 Performance Comparison

In order to evaluate the quality of the prediction of the models the mean absolute percentage error (MAPE) was used: the obtained results are presented in Table 2.2.

$$MAPE = \frac{1}{k} \sum_{i=1}^k \left| \frac{A_i - F_i}{A_i} \right| \cdot 100 \quad (2.6)$$

Table 2.2. Mean absolute percentage error of each model

Model	MAPE
1	57.43 %
2	36.81 %
3	0.42 %

Model 2, thanks to its additional coefficients, is able to outperform model 1 but, as expected, the variable coefficients model yields a much better estimate of the power loss in the *FeSi* lamination; for this reason, together with the ease of evaluation of the variable coefficients, model three will be the target of the FEA implementation procedure.

The visual comparison of the iron loss at $f=50$ Hz, reported in Fig. 2.9, highlights the inability of model 1 and 2 to represent the change in concavity of the loss at increasing magnetic induction. Model 2 performs better than model 1 at $f=400$ Hz, as shown in Fig. 2.10, and both perform poorly at $f=2000$ Hz, as displayed in Fig.

2.11. On the other end, model 3 shows great accuracy at all operating conditions, as suggested by the previous evaluation of a MAPE lower than 1%. The comparison of the estimate for the other two available frequencies is not shown for sake of brevity.

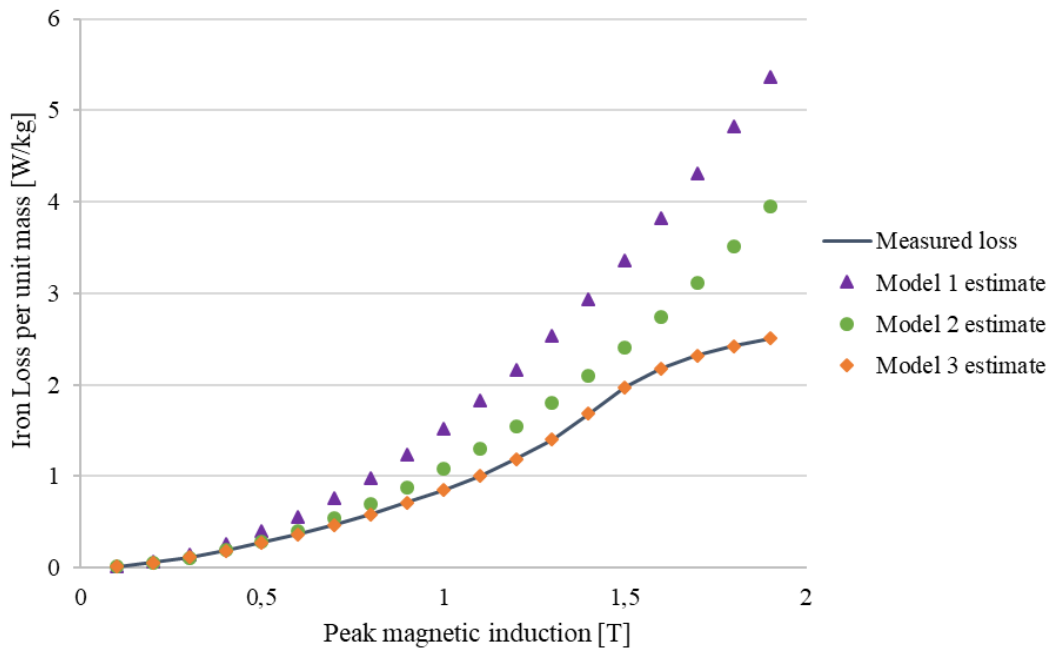


Figure 2.9. Comparison of iron loss estimate of model 1, 2 and 3 at $f=50$ Hz

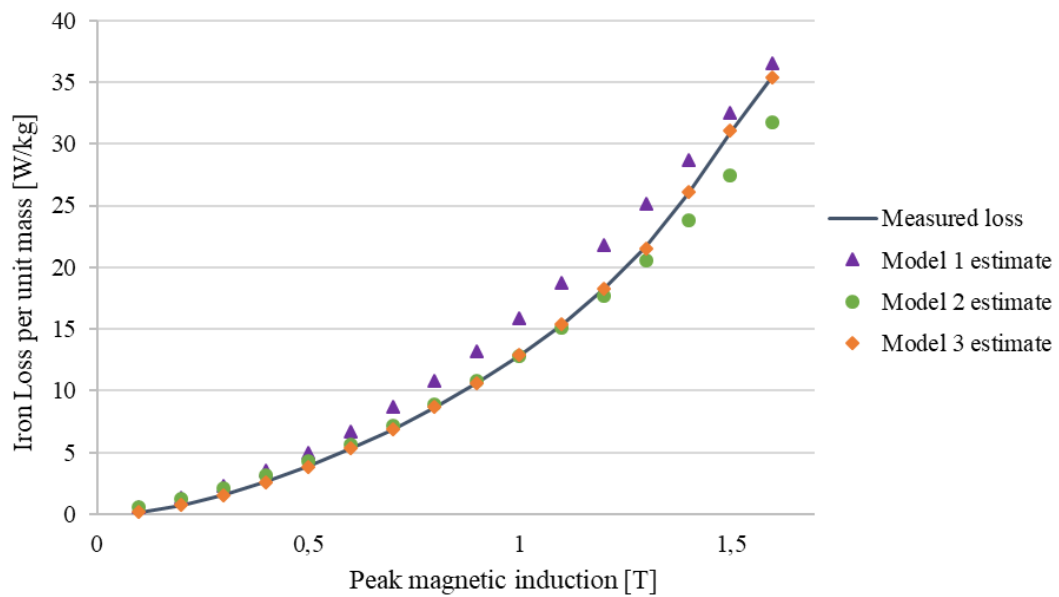


Figure 2.10. Comparison of iron loss estimate of model 1, 2 and 3 at $f=400$ Hz

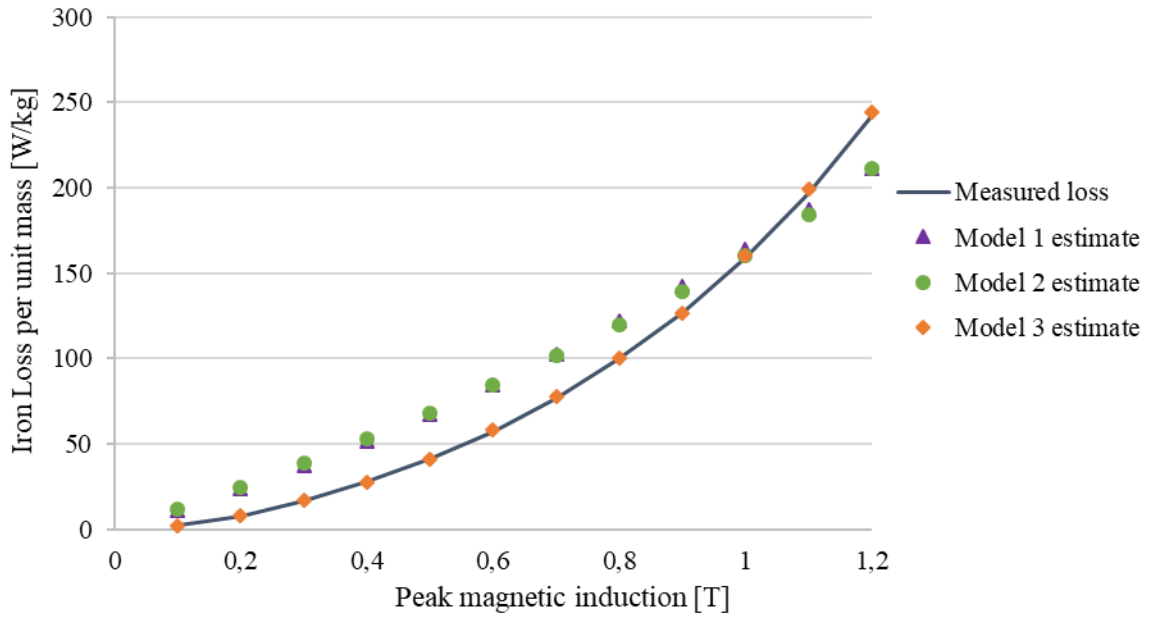


Figure 2.11. Comparison of iron loss estimate of model 1, 2 and 3 at $f=2000$ Hz

2.4 Finite Element Analysis Implementation

In this section, the procedure followed to obtain the iron loss estimate of the IPMSM is explained, starting from the generation of the PWM current input, followed by the definition of an iron loss estimation baseline and concluding with the implementation of the variable coefficients analytical equation, previously mentioned as model 3.

2.4.1 Pulse Width Modulation Currents Generation

The generation of the PWM currents is carried out using the model of the power electronics circuit, previously shown in Figure 2.5. A different current waveform must be obtained for each of the working points available in the iron loss test data; as mentioned earlier, the target value of rotational speed in rpm is directly specified as an input parameter to the simulation whereas the output torque target is controlled by two inputs, I_d and I_q . The values of the d - and q -axis currents are

reported in tables A.3 and A.4 in the Appendix A. The simulation is run for 5 cycles at low rpm values while longer simulations, up to 10 electrical cycles, are required to obtain a stable current at higher speeds. Figures 2.12 and 2.13 show the output of the simulation for two different operating conditions. The transient is discarded and only the values of current of the last electrical cycle are exported to be later used as input in the iron loss simulation.

2.4.2 Iron Loss Baseline Evaluation

A baseline estimate of the iron loss given by Ansys Maxwell™ is required to assess the improvement in prediction accuracy given by the newly developed method. As a baseline, the default iron loss calculation is carried out in Ansys Maxwell™: it uses a time-domain analysis and a constant coefficient analytical model. After having specified to the software the loss curves in the properties of the lamination material, Maxwell evaluates three coefficients K_h , K_c and K_e by fitting the Bertotti iron loss model, based on Eq. (1.16), to the loss curves. For this particular lamination material, in the fitting procedure, the coefficient K_e comes out to be negative, which has no physical meaning. As an alternative Maxwell resorts to using a two-term equation instead, previously referred to as model 1:

$$P_{fe} = K_h f \hat{B}^2 + K_c f^2 \hat{B}^2 \quad (2.7)$$

A new simulation has to be carried out to obtain an estimate of the loss for each speed and torque combination present in the iron loss test data. The first step is to import the correct current waveform into the motor model, previously generated using the PWM circuit model. The simulation time is set-up to 4 electrical cycles due to the first two containing the transient response, which must be discarded.

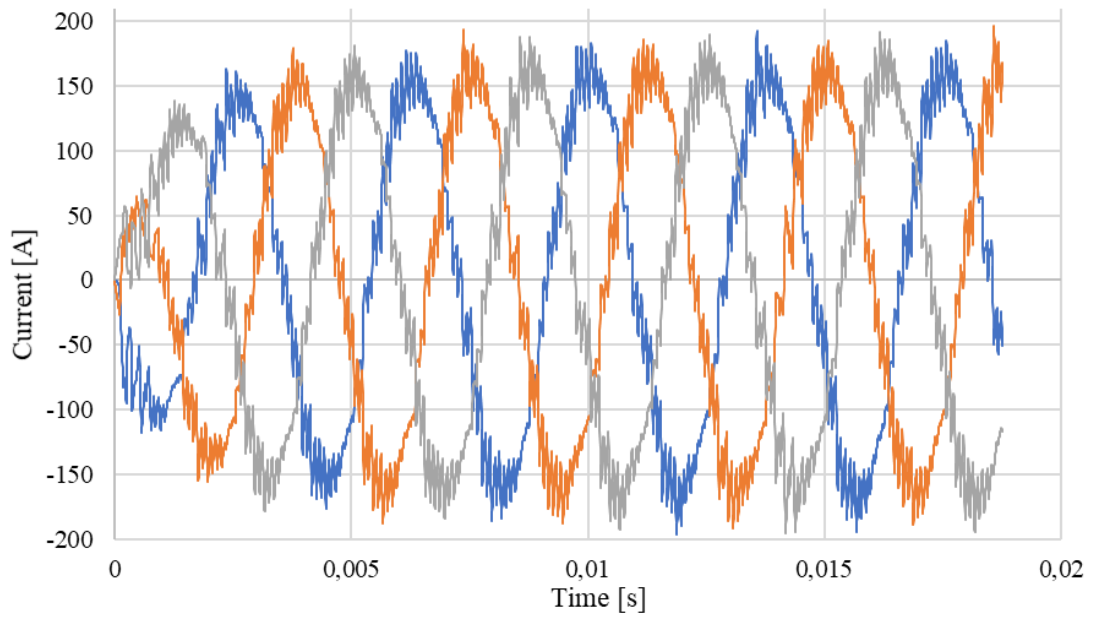


Figure 2.12. PWM currents for $N_s=4000$ rpm and 0.23 pu torque

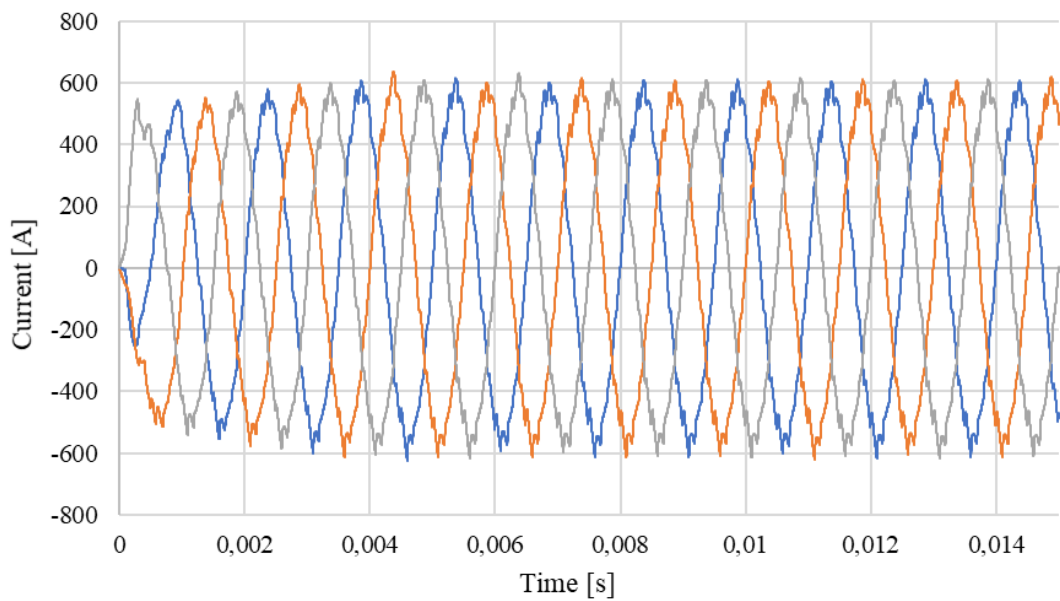


Figure 2.13. PWM currents for $N_s=10000$ rpm and 0.68 pu torque

The correct rotational speed must be specified as input parameter and the simulation can now be run. The output torque is plotted and monitored during the simulation to make sure that the correct operating condition is achieved.

The result of the iron loss estimation is obtained by averaging the instantaneous values of the loss, an example of which is plotted in Fig.2.14, over the last two electrical cycles, both for the stator and the rotor.

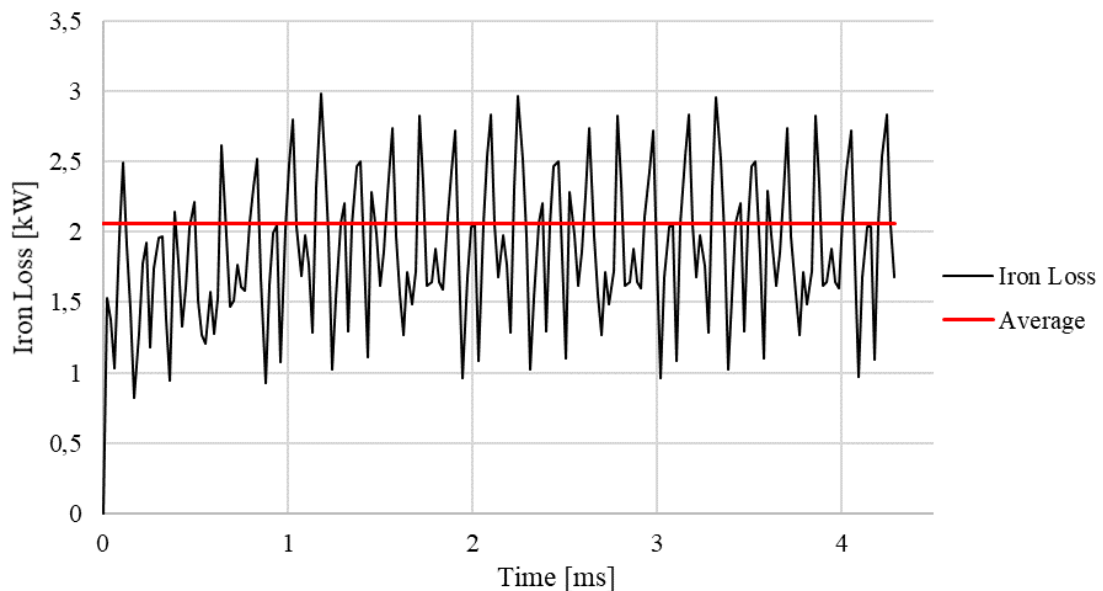


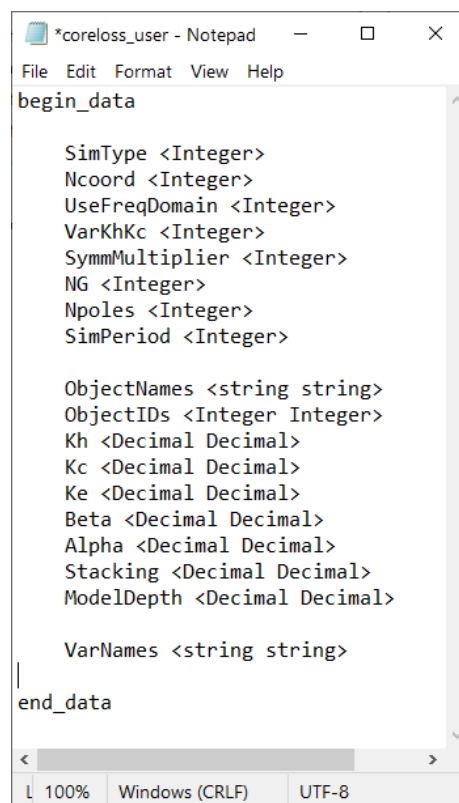
Figure 2.14. Iron loss plot at $N_s=14000$ rpm and 0.5 pu torque

2.4.3 Variable Coefficients Model Implementation

The crucial step of this estimation method resides in the implementation of the variable coefficient model in the FEA software. Unfortunately, this cannot be done directly within Ansys Maxwell™ and an external tool, the *User Defined Core Loss* program, has to be used.

2.4.3.1 User Defined Core Loss Model. The *User Defined Core Loss Model* external program's source code, made available to the author by Ansys, is written in C++ and it's accessible and modifiable by the end user. Its main functionality is controlled via a text file, the *coreloss_user.data* file, whose structure is shown in Figure 2.15. The target of this research is to implement a 2D, frequency-domain, variable coefficient analysis. This is done by setting the following key parameters:

- $N_{coord}=2$
- $UseFreqDomain=1$
- $VarKhKc=1$



```
*coreloss_user - Notepad
File Edit Format View Help
begin_data

  SimType <Integer>
  Ncoord <Integer>
  UseFreqDomain <Integer>
  VarKhKc <Integer>
  SymmMultiplier <Integer>
  NG <Integer>
  Npoles <Integer>
  SimPeriod <Integer>

  ObjectNames <string string>
  ObjectIDs <Integer Integer>
  Kh <Decimal Decimal>
  Kc <Decimal Decimal>
  Ke <Decimal Decimal>
  Beta <Decimal Decimal>
  Alpha <Decimal Decimal>
  Stacking <Decimal Decimal>
  ModelDepth <Decimal Decimal>

  VarNames <string string>
end_data
100% Windows (CRLF) UTF-8
```

Figure 2.15. Coreloss_user.data input file structure

Other important geometry-related parameters include the number of poles of the motor $Npoles$, the lamination stacking factor $Stacking$ and depth of the model in the third direction $ModelDepth$. $SymmMultiplier$ must be correctly specified to account for the fact that, in our case, only $1/8^{th}$ of the cross-section of the motor is modelled. The simulation time (when $SimType=1$) is controlled by the $SimPeriod$ parameter and the integration domain, i.e. the stator and the rotor, must be specified in the $ObjectIDs$ field. Finally, NG controls the number of quadrature integration points.

In a constant coefficient simulation, the solver would read the values of the coefficients of the analytical Iron Loss equation of choice (here named $K_h, K_c, K_e, Beta$ and $Alpha$) directly from the $coreloss_user.data$ file. As it will be explained in the next section, when $VarKhKc=1$, the program requires a separate additional input file containing the values of the variable coefficients $K_h(\hat{B})$ and $K_c(f, \hat{B})$.

2.4.3.2 Implementation Procedure. The first step is to compile the source code of the program, to build an executable file; this was done using Microsoft Visual Studio™. The obtained file is the linked in the *Control Program* field in the advanced section of the solution setup settings in Ansys Maxwell™, as shown in figure 2.16.

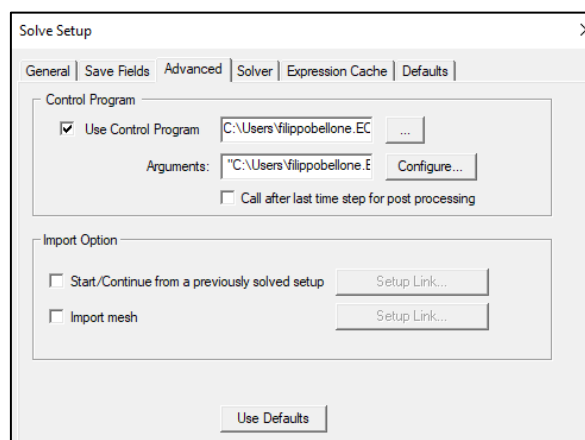


Figure 2.16. Solution setup settings

The directory of the *coreloss_user.data* file, containing the input parameters, must be specified in the arguments field. The list of input parameters used is reported in Table 2.3. In order to run a variable coefficient analysis, an additional input is required by the program: a text file containing the previously evaluated variable coefficients $K_h(\hat{B})$ and $K_c(f, \hat{B})$. This has to be placed in the same directory as the *coreloss_user.data* file.

The correct PWM current, based on the target speed and torque, has to be imported; the currents will be the same as the ones previously used in the baseline iron loss evaluation. Once this is done the simulation can be run, using the external control program. The output of the frequency domain analysis reports the total iron loss, its hysteresis and eddy current loss components, a rotor and stator subdivision and the individual contribution of each harmonic order; an example is shown in Fig. 2.17.

Table 2.3. Variable coefficient analysis input parameters

Parameter	Values	
SimType	1	
Ncoord	2	
UseFreqDomain	1	
VarKhKc	1	
SymmMultiplier	8	
NG	3	
Npoles	8	
SimPeriod	4	
ObjectNames	Stator	Rotor
ObjectIDs	65403	66592
K_h	220.4	220.4
K_c	0.2021	0.2021
K_e	0	0
Alpha	2	2
Beta	0.75	0.75
Stacking	0.95	0.95
ModelDepth	0.105	0.105

Core Losses computed in frequency domain.

Total Loss[W]: 1125.433
Hysteresis Loss[W]: 248.63597
Eddy Loss[W]: 876.79702
Excess Loss[W]: 0

Object Name: Loss:

Stator 972.94012
Rotor 152.49287

Harmonic No.:	Frequency[Hz]:	Total Loss[W]:	Hysteresis Loss[W]:	Eddy Loss[W]:	Excess Loss[W]:
1	533.33	536.04724	191.0577	344.98955	0
2	1066.67	1.535189	0.40595999	1.129229	0
3	1600.00	53.822619	13.0904	40.732219	0
4	2133.33	2.0678915	0.314711	1.7531805	0
5	2666.67	96.404824	15.39827	81.006554	0
6	3200.00	15.940387	2.184692	13.755695	0
7	3733.33	51.161284	6.1802242	44.981059	0
8	4266.67	4.8254227	0.4311408	4.3942819	0
9	4800.00	16.024922	1.5655382	14.459384	0
10	5333.33	0.97302782	0.074135922	0.8988919	0
11	5866.67	7.0107569	0.57272838	6.4380285	0
12	6400.00	75.491152	5.0646878	70.426464	0
13	6933.33	8.500252	0.58316514	7.9170868	0
14	7466.67	11.434252	0.69617324	10.738079	0
15	8000.00	17.682597	0.87205645	16.81054	0
16	8533.33	17.116503	0.91280527	16.203697	0
17	9066.67	11.189932	0.60529875	10.584634	0
18	9600.00	51.684605	2.7376047	48.947	0
19	10133.33	36.547096	1.3465107	35.200585	0
20	10666.67	30.73267	1.4023898	29.330281	0
21	11200.00	7.7386372	0.3512438	7.3873934	0
22	11733.33	13.227185	0.61188897	12.615296	0
23	12266.67	24.884699	0.82790372	24.056795	0
24	12800.00	22.207964	0.90564689	21.302317	0
25	13333.33	11.181884	0.44309611	10.738788	0

Figure 2.17. Iron loss simulation results output file

CHAPTER THREE

IRON LOSS ESTIMATION

In this section the obtained results will be presented, including the absolute iron loss value in Watts estimated by the baseline and variable coefficient models.

3.1 Iron Loss Test Data and Estimations

This section includes the values in Watts of the iron loss measured in the test and estimated by the two models.

3.1.1 Iron Loss Test Data

The measured iron loss of the electric motor, gathered at different torque and speed combinations by FCA, is reported in Table 3.1. As expected, the iron loss increases with increasing torque and speed. The maximum loss is registered when the motor generates 0.5 pu torque at its maximum rotational speed of 14000 rpm, in these conditions the iron loss equals 3297.36 W. This dataset will later be compared to the iron loss estimations of the two models to assess their performance.

3.1.2 Baseline Iron Loss Estimation

Table 3.2 reports the iron loss estimation previously defined as the baseline, obtained using the two-term constant coefficient model employed as the default estimation method by Ansys Maxwell™. Although it is difficult to extrapolate useful information from looking at absolute iron loss values, referencing to the point of maximum loss discussed in the previous section (i.e. 0.5 pu torque at 14000 rpm), a significant drop can be observed, from almost 3300 W to 2057.8 W.

Table 3.1. Iron loss test data

Measured Iron Loss [W]		Speed [rpm]																		
		1000	2000	3000	4000	5000	6000	7000	8000	9000	10000	11000	12000	13000	14000					
Torque/Max Torque	1.00	117.32	269.62	455.43	673.97	924.72	1207.30													
	0.95	114.91	263.51	444.39	656.79	900.23	1174.33	1448.78												
	0.91	112.50	257.42	433.42	639.77	875.99	1141.72	1401.74												
	0.86	110.82	252.93	425.01	626.39	856.60	1115.27	1356.37	1681.61											
	0.82	108.31	246.66	413.79	609.03	831.94	1082.18	1316.11	1603.51											
	0.77	105.88	240.54	402.76	591.89	807.49	1049.22	1279.17	1529.97	1908.36										
	0.73	103.94	235.63	393.89	578.13	787.92	1022.96	1245.37	1465.75	1791.73										
	0.68	101.33	229.19	382.45	560.53	763.04	989.68	1215.50	1407.59	1689.62	2091.17									
	0.64	99.38	224.29	373.66	546.92	743.69	963.69	1187.35	1356.00	1597.39	1938.59	2417.93								
	0.59	96.51	217.27	361.25	527.92	716.92	927.98	1158.72	1306.31	1517.21	1808.67	2206.08	2743.00							
	0.55	94.66	212.70	353.14	515.45	699.31	904.44	1130.67	1264.51	1443.00	1695.39	2025.60	2457.16	3043.14						
	0.50	91.37	204.72	339.13	494.11	669.33	864.56	1079.63	1224.31	1380.70	1590.34	1871.14	2230.59	2695.43	3297.36					
	0.45	89.15	199.34	329.68	479.70	649.11	837.65	1045.18	1189.67	1320.29	1501.60	1734.07	2036.96	2414.58	2890.72					
	0.41	85.72	191.10	315.30	457.91	618.62	797.23	993.57	1159.45	1268.51	1415.48	1619.13	1867.51	2184.35	2564.54					
	0.36	82.87	184.26	303.42	439.92	593.50	763.95	951.13	1130.34	1217.97	1346.54	1510.15	1724.84	1985.98	2303.14					
	0.32	80.05	177.59	291.87	422.51	569.26	731.92	910.35	1101.89	1177.32	1276.99	1420.51	1593.72	1813.07	2076.65					
	0.27	75.65	167.17	273.87	395.43	531.60	682.21	847.14	1026.24	1138.49	1225.08	1333.62	1480.35	1665.23	1883.88					
	0.23	71.93	158.43	258.88	372.97	500.48	641.25	795.17	962.08	1106.07	1167.97	1263.68	1383.67	1532.39	1720.66					
	0.18	68.19	149.71	244.00	350.77	469.84	601.04	744.29	899.45	1066.23	1132.72	1198.37	1296.72	1427.89	1577.44					
	0.14	64.04	140.11	227.69	326.53	436.44	557.29	688.98	831.40	984.50	1087.41	1148.19	1231.00	1332.34	1466.58					
0.09	60.85	132.82	215.42	308.43	411.66	525.00	648.35	781.61	924.72	1072.64	1109.69	1174.88	1269.18	1378.63						
0.05	57.88	126.03	204.00	291.58	388.60	494.94	610.53	735.26	869.10	1011.94	1085.05	1145.69	1223.31	1325.41						
0.00	57.29	124.68	201.76	288.30	384.13	489.15	603.27	726.39	858.46	999.40	1081.17	1139.86	1214.15	1312.61						

More in depth analysis of the prediction accuracy of this estimation method will be given in the following sections, looking at percentage error and MAPE.

3.1.3 Variable Coefficients Model Iron Loss Estimation

The iron loss estimate, obtained using the newly implemented method, is reported in Table 3.3; from here on out the model will be referred to as *VarKhKc* for sake of brevity. Once again, when looking at the working point associated to the maximum iron loss, this model quite accurately estimates it at 3287.35 W, compared to the test 3297.36 W.

3.2 Second Motor Analysis Setup

To validate the estimation procedure and verify its consistency, the iron loss estimation method needs to be tested on different electric motors. Although multiple motors would be the preferred choice, the unavailability of test data and extremely time-consuming simulations required allowed the implementation of this method on a single other electric motor. This section includes a description of the second motor analyzed, the data and models required for implementation and a brief explanation of the methodology followed to estimate the iron loss, analogue to the one explained in Chapter 2. In conclusion, the analysis of the obtained results and a comparison with the previously obtained results on the first motor will be presented.

To perform the analysis, two Ansys models are required: the 2D model of the motor and the PWM currents generation model; both were provided by FCA, alongside the iron loss test data measured on the motor.

Table 3.2. Baseline model iron loss estimate

Baseline Model Iron Loss Estimate [W]		Speed [rpm]																	
		1000	2000	3000	4000	5000	6000	7000	8000	9000	10000	11000	12000	13000	14000				
Torque/Max Torque	1.00	83.93	199.67	341.80	453.60	575.20	716.70												
	0.95	79.78	192.05	328.85	443.30	553.40	700.40	825.00											
	0.91	76.06	175.86	322.14	442.90	552.10	683.50	818.00											
	0.86	79.02	173.92	338.40	435.90	550.40	673.70	793.50	962.70										
	0.82	74.96	162.33	316.76	411.80	540.40	654.80	775.60	931.00										
	0.77	75.87	158.98	364.64	405.30	511.60	644.10	763.80	898.00	1120.90									
	0.73	76.59	154.19	331.32	391.40	497.20	630.70	757.60	861.30	1073.20									
	0.68	75.35	152.36	286.90	357.20	477.80	600.70	749.80	833.40	1004.90	1209.10								
	0.64	72.14	147.57	280.70	350.46	469.10	590.10	734.00	802.70	960.90	1163.90	1454.60							
	0.59	69.50	144.23	257.06	337.92	448.20	559.50	714.50	773.00	908.80	1101.80	1325.60	1660.30						
	0.55	66.00	142.80	235.72	322.37	439.90	552.10	700.60	753.30	858.70	1030.10	1230.70	1517.60	1856.90					
	0.50	63.63	134.24	215.12	302.87	416.39	516.69	672.60	728.50	830.00	985.90	1170.60	1388.20	1676.00	2057.80				
	0.45	63.09	130.70	219.29	295.00	404.75	499.01	645.20	712.50	805.10	949.20	1096.30	1279.00	1528.80	1819.50				
	0.41	58.72	118.68	199.49	276.88	375.05	466.41	609.40	692.50	782.40	894.80	1012.40	1176.40	1362.50	1613.80				
	0.36	58.75	113.13	195.32	268.19	369.21	454.69	593.10	690.80	765.70	865.30	971.00	1115.90	1266.60	1496.70				
	0.32	54.52	111.72	182.87	253.65	350.90	435.30	569.30	686.70	747.40	833.70	934.30	1063.60	1184.30	1392.10				
	0.27	50.44	104.41	169.56	242.08	331.61	410.93	539.40	662.50	727.20	816.70	897.10	1012.50	1126.60	1314.10				
	0.23	51.88	97.88	158.08	225.74	315.08	392.17	515.60	636.50	708.40	781.80	866.40	958.00	1056.00	1230.40				
	0.18	45.12	91.08	147.59	209.77	291.39	356.04	479.70	602.80	671.10	749.00	822.20	907.50	986.80	1159.80				
	0.14	43.56	85.62	130.83	191.11	266.57	323.72	445.40	545.40	623.20	713.30	794.50	845.40	932.40	1087.60				
0.09	40.16	76.86	119.96	174.99	244.96	290.48	408.54	492.20	567.20	667.80	746.10	791.90	858.10	1019.70					
0.05	37.43	66.81	102.67	154.66	220.08	257.70	370.42	442.05	521.10	620.20	684.50	735.80	810.70	952.90					
0.00	25.38	55.47	90.27	129.79	174.03	222.96	276.57	334.99	397.71	465.87	538.35	615.57	697.49	783.47					

Table 3.3. Variable coefficients model iron loss estimate

VarKhKc Model Iron Loss Estimate [W]		Speed [rpm]																	
		1000	2000	3000	4000	5000	6000	7000	8000	9000	10000	11000	12000	13000	14000				
Torque/Max Torque	1.00	100.94	260.86	463.39	665.91	766.52	965.79												
	0.95	82.95	244.53	437.76	630.99	749.84	937.85	1221.90											
	0.91	71.03	210.44	404.15	597.85	746.14	915.62	1210.17											
	0.86	87.03	202.95	377.21	551.47	746.85	899.62	1168.05	1411.49										
	0.82	70.02	175.17	350.51	525.85	746.32	874.00	1123.20	1368.47										
	0.77	87.58	172.06	350.78	529.50	707.95	873.46	1114.29	1326.68	1653.08									
	0.73	92.75	162.96	359.32	555.68	686.74	846.66	1108.66	1270.66	1598.81									
	0.68	81.62	161.32	333.85	506.39	664.43	794.89	1109.78	1233.30	1485.99	1821.19								
	0.64	83.63	155.67	302.97	450.27	639.16	784.43	1074.35	1178.94	1423.05	1752.39	2223.89							
	0.59	75.37	155.60	294.43	433.25	604.36	727.87	1040.00	1125.43	1332.39	1659.60	1990.80	2491.40						
	0.55	64.35	149.62	271.57	393.51	616.49	725.83	1020.86	1086.12	1243.25	1535.28	1837.31	2271.10	3111.03					
	0.50	62.68	143.65	249.99	356.32	570.82	659.65	988.92	1037.06	1202.47	1457.92	1768.29	2072.29	2800.45	3285.37				
	0.45	63.45	138.25	248.60	358.94	553.12	636.13	945.93	1006.06	1150.57	1414.92	1619.67	1899.94	2541.25	2788.23				
	0.41	60.27	120.07	222.98	325.89	515.34	583.00	906.12	973.66	1115.57	1312.18	1467.89	1736.83	2237.26	2473.55				
	0.36	70.64	109.79	215.80	321.80	506.92	574.07	880.77	979.73	1094.73	1259.08	1392.92	1642.95	2033.99	2286.99				
	0.32	51.12	107.84	195.27	282.70	473.97	542.20	824.61	977.56	1056.72	1200.84	1337.53	1558.83	1868.05	1947.86				
	0.27	46.57	98.76	188.63	278.49	442.57	501.73	780.56	961.18	1020.95	1180.59	1275.46	1463.87	1754.45	1787.04				
	0.23	54.83	90.01	166.24	242.47	410.84	477.57	754.40	930.57	983.13	1122.45	1225.21	1389.72	1616.75	1727.06				
	0.18	40.14	86.57	156.07	225.57	380.43	414.67	697.72	888.36	922.31	1084.86	1161.96	1302.99	1478.29	1608.73				
	0.14	42.82	83.97	144.05	204.13	349.02	366.94	649.25	787.54	871.38	1013.33	1141.54	1210.49	1405.40	1497.05				
0.09	41.10	74.99	131.75	188.52	320.92	327.00	608.90	698.84	794.29	947.99	1084.31	1136.71	1298.89	1414.91					
0.05	41.32	66.00	119.63	173.25	294.71	300.13	563.37	644.33	762.93	896.00	976.31	1051.81	1248.22	1348.37					
0.00	19.75	49.15	91.50	133.84	189.63	241.86	317.43	381.29	471.87	550.02	637.01	734.55	903.43	985.35					

3.2.1 Finite Element Analysis Model

The second motor under analysis, whose 2D section is reported in Fig. 3.1, is once again an interior permanent magnet synchronous motor; it has 8 poles, 48 slots and v-shaped buried $Nd_2Fe_{14}B$ magnets. Differences from the previous motor include a bigger size, different magnet and stator winding configurations, higher torque and power output and, most importantly, a different lamination material with reduced lamination thickness. The base speed is 4600 rpm, and the maximum speed of the motor is 16000 rpm; torque and power values cannot be disclosed and will be expressed on a per unit base.

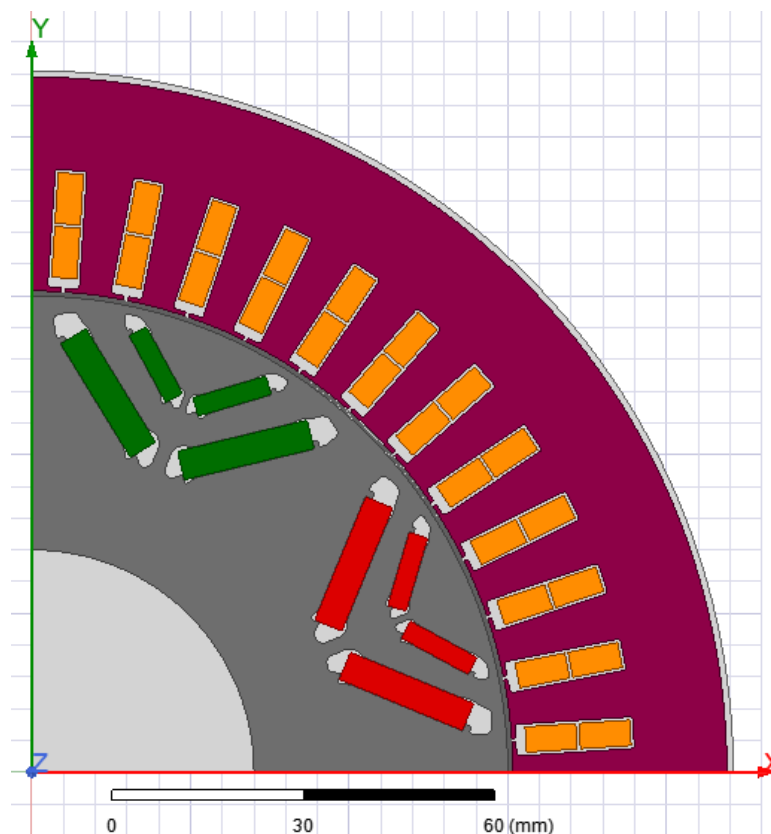


Figure 3.1. Ansys Maxwell™ 2D model of the second IPMSM

3.2.2 Pulse Width Modulation Current Generation Model

The model used to generate the PWM input currents is reported in Fig. 3.2, it includes the 3-phase inverter, the equivalent circuit model of the motor and the PWM controller. Following the same methodology employed for the first motor, the PWM model is used to generate a new current waveform corresponding to the speed-torque operating point to be analyzed, according to the specified I_d and I_q values, reported in Tables A.5 and A.6 in the Appendix A.

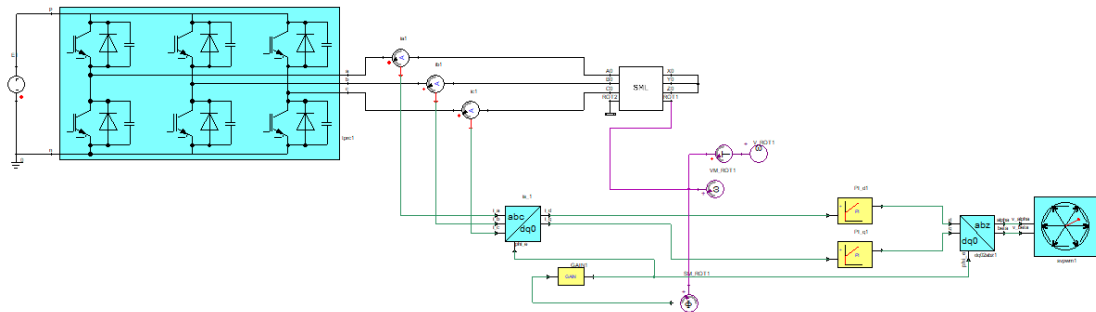


Figure 3.2. PWM current generation model of the second IPMSM

3.2.3 Coreloss_user.data Input File and Variable Coefficients Evaluation

In addition to the PWM current, the variable coefficient simulation requires two input files to run, one containing the input parameters and the other containing the variable coefficients. The first, containing the input parameters, is shown in Table 3.4. With respect to the first motor, the parameters that needed modification are the *SymmMultiplier*, now equal to 4, and the ID of the stator and rotor objects.

Table 3.4. Variable coefficient analysis input file of the second IPMSM

Parameter	Values	
SimType	1	
Ncoord	2	
UseFreqDomain	1	
VarKhKc	1	
SymmMultiplier	4	
NG	3	
Npoles	8	
SimPeriod	4	
ObjectNames	Stator	Rotor
ObjectIDs	254644	289929
K_h	283.07	283.07
K_c	0.15124	0.15124
K_e	0	0
Alpha	2	2
Beta	0.75	0.75
Stacking	0.95	0.95
ModelDepth	0.150	0.150

The different lamination material used in the core of the machine requires a new evaluation of the variable $K_h(\hat{B})$ and $K_c(f, \hat{B})$ coefficients, this is done starting from the loss curves of the lamination material, plotted in Fig. 3.3.

The lamination material iron loss information, together with the material density of 7600 kg/m^3 , are given as input to the python script of the *Extract Core Loss Coefficients* toolkit and the variable coefficients are obtained, as explained in section 2.3.3. The output .txt file containing the coefficients is placed in the same directory of the *coreloss_user.data* file as the last input required to run the simulations.

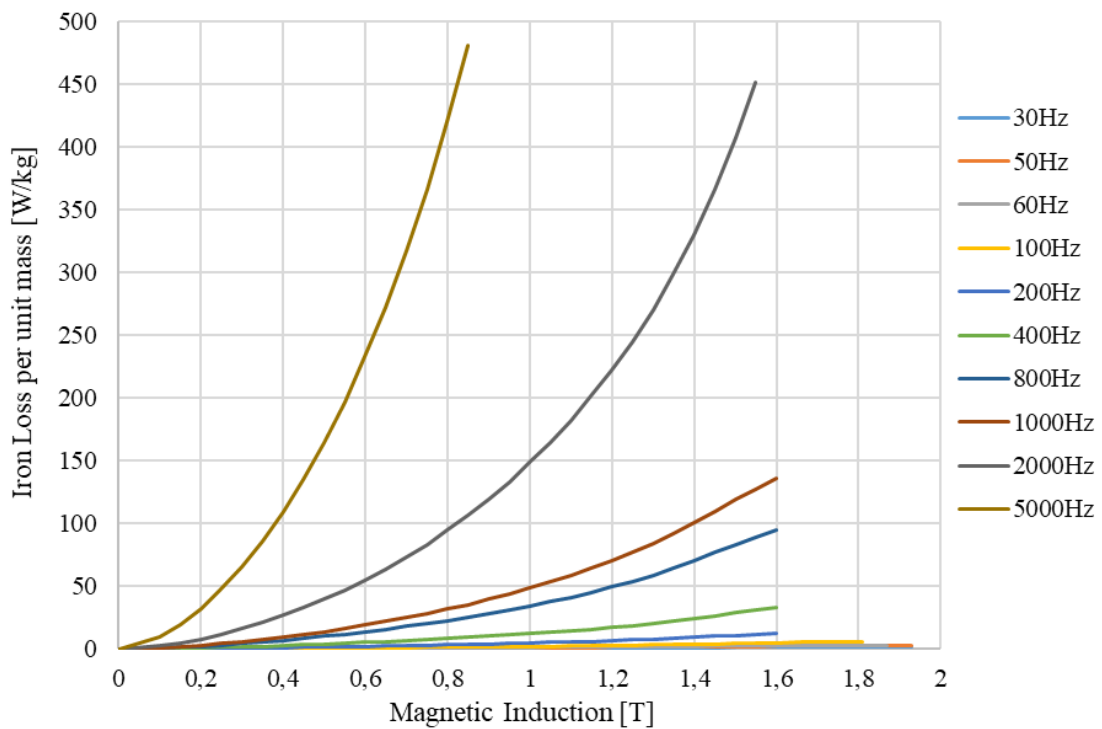


Figure 3.3. Iron loss per unit mass as function of magnetic induction at different magnetization frequencies of the lamination material of the second motor

3.3 Iron Loss Test Data and Estimations on the Second Motor

This section includes the values in Watts of the iron loss measured in the test and estimated by the two models. Given the much higher maximum torque with respect to the first motor and the even longer computational time, caused by the modelling of $1/4^{\text{th}}$ of the cross-section with respect to $1/8^{\text{th}}$ of the first motor, the simulations were carried out at larger torque intervals and 800 rpm speed intervals.

3.3.1 Iron Loss Test Data of the Second Motor

The iron loss test data, reported in Table 3.5, follows the expected behavior, where the loss is increasing at higher values of torque and rotational speed. The maximum iron loss is registered at the highest achievable torque and the maximum rotational speed of the motor (i.e. 0.22 pu torque at 16000 rpm) and it is measured at 3404.28 W.

This dataset will later be compared to the iron loss estimations of the two models to assess their performance.

3.3.2 Baseline Model Iron Loss Estimate on the Second Motor

The estimate of the iron loss of the motor, obtained using the default model implemented in Ansys Maxwell™, is reported in Table 3.6. The overall trend of the loss is consistent, making exception of the estimate at no-load, which in the higher rpm range shows higher values than the ones simulated at higher torque values, which is unreasonable. This can be attributed to the methodology employed to simulate the no-load condition, which may lead to inconsistent results at higher rotational speeds.

Looking at the reference point of maximum loss, it is immediately possible to notice a significant discrepancy, as the estimation is over two kilowatts lower than the test results. Better analysis of the overall performance of the model will be given when looking at the percentage errors in the next sections.

3.3.3 Variable Coefficients Model Iron Loss Estimate on the Second Motor

The iron loss estimate, obtained using the variable coefficient model, is presented in Table 3.7. The loss table shows high discrepancy in the lower speed region, especially in the range between 1600 rpm and 3200 rpm. The loss estimated at the speeds of 2400 and 3200 rpm are lower than the one evaluated at 1600 rpm, highlighting an unrealistic trend inversion. This could be caused either by an overestimation at the lower speed or from an underestimation at the two higher speeds and will be further investigated in the next sections.

When looking at the reference point of maximum loss (0.22 pu torque at 16000 rpm), the variable coefficient model shows a massive performance improvement over the baseline, estimating the loss at 2575.93 W, more than 1200 W closer to the actual loss measured on the motor. Further analysis of the performance of the model in all the different operating conditions is given in the next sections, looking at the percentage errors.

Table 3.5. Iron loss test data of second IPMSM

Measured Iron Loss [W]	Speed [rpm]																			
	800	1600	2400	3200	4000	4800	5600	6400	7200	8000	8800	9600	10400	11200	12000	12800	13600	14400	15200	16000
1.00	273.14	502.65	702.99	962.79	1060.08															
0.95	264.63	486.86	680.78	932.28	1026.59	1255.93														
0.90	256.08	470.99	658.43	901.59	992.90	1199.31														
0.85	247.82	455.68	636.87	871.99	960.40	1148.08														
0.80	239.44	440.11	614.95	841.89	927.35	1100.88	1408.32													
0.76	231.35	425.10	593.83	812.88	895.53	1056.78	1331.90													
0.71	223.38	410.33	573.03	784.32	864.16	1014.90	1266.34	1613.09												
0.66	215.50	395.69	552.43	756.02	833.12	975.07	1207.31	1504.03												
0.61	207.78	381.36	532.25	728.32	802.68	936.86	1152.76	1419.60	1756.97											
0.56	199.83	366.61	511.48	699.79	771.36	900.09	1101.20	1346.29	1631.36	2071.62										
0.51	192.18	352.43	491.52	672.38	741.28	864.77	1052.16	1279.50	1535.16	1836.03										
0.46	184.49	338.15	471.41	644.78	710.96	830.58	1004.87	1217.13	1451.91	1714.18	2003.30									
0.41	176.72	323.73	451.12	616.91	680.37	797.71	959.09	1157.75	1375.88	1614.01	1861.10	2109.06								
0.37	169.05	309.49	431.07	589.39	650.14	765.50	914.68	1100.51	1304.54	1524.69	1748.47	1959.87	2173.47	2423.72						
0.32	161.15	294.83	410.42	561.03	619.01	732.32	871.23	1044.82	1236.29	1441.85	1649.23	1842.11	2028.15	2218.33	2434.76	2780.05				
0.27	153.38	280.42	390.14	533.18	588.43	699.73	829.38	990.16	1170.10	1363.20	1557.87	1738.52	1910.33	2081.29	2267.56	2533.44	2811.70	3075.89		
0.22	145.28	265.38	368.96	504.10	556.49	665.70	789.02	936.18	1105.12	1287.36	1471.91	1643.72	1806.63	1967.06	2139.75	2382.69	2630.20	2847.25	3062.61	3404.28
0.17	136.94	249.90	347.16	474.18	523.64	630.69	749.80	882.59	1040.59	1213.47	1389.94	1555.75	1712.84	1866.49	2031.56	2261.22	2493.52	2694.73	2890.32	3196.84
0.12	128.22	233.72	324.38	442.91	489.29	594.10	708.99	829.64	975.93	1141.18	1312.44	1474.83	1628.35	1778.59	1939.65	2159.91	2382.33	2574.77	2761.11	3050.48
0.07	118.76	216.15	299.64	408.95	452.00	554.37	664.68	778.38	910.82	1072.94	1242.62	1404.21	1557.83	1706.84	1865.46	2080.42	2298.26	2485.93	2665.93	2943.51
0.02	108.52	197.14	272.87	372.20	411.65	511.39	616.74	724.81	849.84	1019.20	1193.42	1357.98	1510.45	1660.35	1820.60	2032.80	2247.98	2431.12	2609.11	2881.49
0.00	102.47	185.97	257.19	350.51	387.96	485.93	588.11	692.56	797.41	901.46	1006.24	1107.81	1204.50	1299.84	1405.55	1549.37	1697.06	1824.24	1943.17	2123.03

Table 3.6. Baseline iron loss estimate on the second IPMSM

Baseline Model Iron Loss Estimate [W]	Speed [rpm]																			
	800	1600	2400	3200	4000	4800	5600	6400	7200	8000	8800	9600	10400	11200	12000	12800	13600	14400	15200	16000
1.00	134.89	276.61	431.88	592.32	763.10															
0.95	132.92	267.10	424.04	578.19	749.70	864.30														
0.90	130.54	263.52	411.23	562.16	741.00	830.40														
0.85	127.74	255.50	399.39	546.27	720.80	795.20														
0.80	122.22	251.88	391.68	534.51	704.40	786.00	861.30													
0.76	117.17	242.13	378.83	515.59	682.50	770.00	829.70													
0.71	117.14	233.56	367.34	498.09	662.20	754.90	797.20	904.30												
0.66	113.05	228.26	359.14	489.97	650.60	749.30	785.90	838.00												
0.61	107.01	217.88	338.82	467.74	624.87	733.50	772.70	801.00	866.80											
0.56	105.27	213.11	331.80	445.88	599.37	718.30	756.50	776.10	843.70	871.90										
0.51	104.76	208.86	326.37	426.29	582.96	703.40	734.80	773.10	788.80	842.90										
0.46	101.81	204.13	318.81	420.18	563.16	683.20	725.50	738.80	774.20	810.90	899.90									
0.41	97.49	195.34	306.13	401.12	526.93	657.80	706.30	738.00	766.90	784.10	865.50	909.40								
0.37	94.77	182.37	287.98	393.15	518.04	638.70	690.30	692.20	728.80	749.70	798.80	871.00	946.10	1014.90						
0.32	84.50	164.78	266.62	360.46	471.34	591.60	660.50	660.70	680.09	711.90	743.80	795.30	911.10	982.50	1001.20	1086.20				
0.27	81.78	161.83	248.53	331.65	438.14	550.44	622.40	633.50	641.61	655.90	692.70	723.40	826.70	866.30	951.10	1041.00	1182.00	1196.30		
0.22	77.68	147.70	226.91	308.77	399.84	507.93	576.90	607.25	604.75	614.04	654.44	671.30	725.50	786.80	840.10	959.00	1020.10	1125.20	1237.40	1313.00
0.17	68.92	127.90	201.25	264.10	381.23	482.53	537.65	583.16	581.58	583.29	596.55	623.74	666.78	715.00	762.80	869.40	906.10	985.40	1074.40	1167.30
0.12	62.13	113.52	172.20	244.91	337.68	420.73	503.65	553.76	546.80	548.19	570.17	571.44	629.89	662.90	696.90	795.10	835.40	889.60	979.30	1074.90
0.07	52.15	112.72	156.25	213.05	277.79	353.13	427.61	495.56	519.14	527.01	531.18	556.08	588.39	608.83	647.80	743.20	772.00	827.80	896.50	979.30
0.02	47.06	80.39	135.50	185.32	240.48	307.41	378.93	440.70	507.22	519.49	513.39	534.89	562.24	585.85	621.63	701.80	736.30	780.10	847.00	920.10
0.00	37.65	78.03	121.15	167.01	215.61	266.95	321.02	377.82	437.39	499.67	564.99	632.54	703.00	776.24	852.19	930.90	1012.40	1096.60	1183.60	1273.20

Table 3.7. VarKhKc iron loss estimate on the second IPMSM

VarKhKc Model Iron Loss Estimate [W]	Speed [rpm]																			
	800	1600	2400	3200	4000	4800	5600	6400	7200	8000	8800	9600	10400	11200	12000	12800	13600	14400	15200	16000
1.00	188.52	460.78	274.85	418.88	582.46															
0.95	186.49	475.24	270.65	411.21	574.60	728.11														
0.90	181.39	430.85	263.32	404.47	571.10	711.50														
0.85	164.20	439.07	259.40	395.99	561.29	689.40														
0.80	154.07	449.15	258.01	390.27	549.71	672.48	891.70													
0.76	153.10	435.77	250.50	377.86	535.68	657.34	871.63													
0.71	144.13	375.35	244.99	368.23	523.08	644.93	855.18	1065.42												
0.66	156.14	397.94	241.48	364.71	515.40	637.79	817.51	997.24												
0.61	142.47	405.64	230.03	351.10	498.76	625.30	772.66	920.01	1060.02											
0.56	140.80	329.06	225.69	333.93	479.83	612.26	729.84	847.42	1016.73	1053.49										
0.51	135.07	402.41	222.14	320.85	467.21	598.54	727.88	857.21	912.19	1029.29										
0.46	127.74	329.96	217.77	316.74	452.45	583.18	676.59	770.00	866.26	955.29	1233.32									
0.41	127.27	317.09	210.14	302.55	425.75	560.23	692.98	825.73	850.19	949.44	1200.31	1203.98								
0.37	124.75	322.25	199.44	297.58	418.02	543.37	610.19	677.01	790.52	945.10	1124.98	1177.96	1369.99	1537.18						
0.32	115.26	255.57	185.17	272.96	384.48	506.79	573.90	641.01	745.10	929.99	1067.47	1087.89	1305.26	1510.54	1614.34	2342.42				
0.27	112.31	252.71	174.18	251.05	354.83	471.67	543.91	616.15	678.11	862.85	1023.40	958.25	1210.86	1380.27	1543.14	2265.12	2306.92	2224.82		
0.22	108.30	245.48	156.87	230.19	321.32	431.75	519.72	607.68	635.96	750.10	975.65	907.73	1129.52	1304.66	1420.07	1974.91	2087.45	2123.16	2419.78	2575.93
0.17	104.22	197.65	130.97	190.79	300.71	404.13	489.90	575.67	614.30	665.24	876.71	826.56	1092.95	1242.62	1319.03	1851.06	1902.92	1891.42	2033.42	2313.08
0.12	90.78	163.64	112.36	170.44	252.71	335.46	436.93	538.40	565.77	604.15	838.81	755.72	1101.30	1196.58	1228.51	1698.79	1776.41	1734.89	1833.30	2061.91
0.07	73.05	158.80	100.48	143.93	202.85	272.31	379.38	486.46	567.68	655.96	837.63	856.83	1024.76	1160.98	1191.55	1570.24	1658.44	1622.97	1659.07	1933.08
0.02	69.16	136.25	87.37	125.86	174.87	243.46	336.20	428.93	594.24	686.50	837.24	829.42	1005.96	1196.53	1211.43	1520.97	1607.36	1575.87	1627.05	1880.65
0.00	53.41	121.65	73.57	117.58	161.06	210.30	266.91	323.51	390.81	464.97	553.17	648.11	747.13	846.65	946.79	1061.73	1189.62	1291.81	1383.18	1560.14

CHAPTER FOUR

ANALYSIS OF RESULTS AND DISCUSSION

4.1 Performance Analysis on the First Motor

In this section the percentage difference of each estimation with respect to the test data will be presented and analyzed, together with a comparison of the prediction errors of the two estimation methods; it must be kept in mind that the accuracy of the test data is estimated at $\pm 5\%$. Furthermore, the data will be analyzed focusing on two different speed ranges to highlight the estimation behavior of the newly implemented method.

4.1.1 Baseline Model Performance Analysis on the First Motor

From the percentage difference between the baseline model estimate and the test data, reported in Table 4.1, it can be immediately noticed a heavy underestimation of the iron loss in the motor across the entire set of possible operating conditions. The estimation error is almost constant across different speeds denoting a quite consistent, although poor, estimation. The bigger estimation errors are encountered at no-load, which has been simulated without any currents in the excitations; here percentage errors above 50% are observed, especially in the lower rpm region.

4.1.2 Variable Coefficients Model Performance Analysis on the First Motor

The results shown in Table 4.2 highlight a quite significant behavior of the VarKhKc model with respect to the baseline model, showing an improved estimation performance. Once again, the prediction generally underestimates the iron loss in the motor, but by a lower amount across the board, whereas a few operating points near the maximum speed slightly overestimate the loss. Similar performance to the baseline model

Table 4.1. Percentage error of the baseline model estimation

Percentage Error - Baseline Model		Speed [rpm]																		
		1000	2000	3000	4000	5000	6000	7000	8000	9000	10000	11000	12000	13000	14000					
Torque/Max Torque	1.00	-28.46	-25.94	-24.95	-32.70	-37.80	-40.64													
	0.95	-30.58	-27.12	-26.00	-32.51	-38.53	-40.36	-43.06												
	0.91	-32.39	-31.69	-25.67	-30.77	-36.97	-40.13	-41.64												
	0.86	-28.69	-31.24	-20.38	-30.41	-35.75	-39.59	-41.50	-42.75											
	0.82	-30.80	-34.19	-23.45	-32.38	-35.04	-39.49	-41.07	-41.94											
	0.77	-28.34	-33.91	-9.47	-31.52	-36.64	-38.61	-40.29	-41.31	-41.26										
	0.73	-26.31	-34.56	-15.89	-32.30	-36.90	-38.35	-39.17	-41.24	-40.10										
	0.68	-25.64	-33.52	-24.98	-36.27	-37.38	-39.30	-38.31	-40.79	-40.53	-42.18									
	0.64	-27.42	-34.21	-24.88	-35.92	-36.92	-38.77	-38.18	-40.80	-39.85	-39.96	-39.84								
	0.59	-27.99	-33.62	-28.84	-35.99	-37.48	-39.71	-38.34	-40.83	-40.10	-39.08	-39.91	-39.47							
	0.55	-30.28	-32.86	-33.25	-37.46	-37.10	-38.96	-38.04	-40.43	-40.49	-39.24	-39.24	-38.24	-38.98						
	0.50	-30.36	-34.43	-36.57	-38.70	-37.79	-40.24	-37.70	-40.50	-39.89	-38.01	-37.44	-37.77	-37.82	-37.59					
	0.45	-29.23	-34.43	-33.48	-38.50	-37.64	-40.43	-38.27	-40.11	-39.02	-36.79	-36.78	-37.21	-36.68	-37.06					
	0.41	-31.50	-37.90	-36.73	-39.53	-39.37	-41.50	-38.67	-40.27	-38.32	-36.78	-37.47	-37.01	-37.62	-37.07					
	0.36	-29.10	-38.60	-35.63	-39.04	-37.79	-40.48	-37.64	-38.89	-37.13	-35.74	-35.70	-35.30	-36.22	-35.01					
	0.32	-31.90	-37.09	-37.34	-39.96	-38.36	-40.53	-37.46	-37.68	-36.52	-34.71	-34.23	-33.26	-34.68	-32.96					
	0.27	-33.33	-37.54	-38.09	-38.78	-37.62	-39.77	-36.33	-35.44	-36.13	-33.33	-32.73	-31.60	-32.35	-30.25					
	0.23	-27.88	-38.22	-38.94	-39.48	-37.04	-38.84	-35.16	-33.84	-35.95	-33.06	-31.44	-30.76	-31.09	-28.49					
	0.18	-33.83	-39.16	-39.51	-40.20	-37.98	-40.76	-35.55	-32.98	-37.06	-33.88	-31.39	-30.02	-30.89	-26.48					
	0.14	-31.99	-38.89	-42.54	-41.47	-38.92	-41.91	-35.35	-34.40	-36.70	-34.40	-30.80	-31.32	-30.02	-25.84					
0.09	-34.01	-42.13	-44.31	-43.26	-40.50	-44.67	-36.99	-37.03	-38.66	-37.74	-32.76	-32.60	-32.39	-26.04						
0.05	-35.33	-46.98	-49.67	-46.96	-43.37	-47.93	-39.33	-39.88	-40.04	-38.71	-36.92	-35.78	-33.73	-28.11						
0.00	-55.70	-55.51	-55.26	-54.98	-54.70	-54.42	-54.15	-53.88	-53.67	-53.38	-50.21	-46.00	-42.55	-40.31						

Table 4.2. Percentage error of the VarKhKc model estimation

Percentage Error - VarKhKc Model		Speed [rpm]																		
		1000	2000	3000	4000	5000	6000	7000	8000	9000	10000	11000	12000	13000	14000					
Torque/Max Torque	1.00	-13.96	-3.25	1.75	-1.19	-17.11	-20.00													
	0.95	-27.81	-7.20	-1.49	-3.93	-16.71	-20.14	-15.66												
	0.91	-36.86	-18.25	-6.75	-6.55	-14.82	-19.80	-13.67												
	0.86	-21.46	-19.76	-11.25	-11.96	-12.81	-19.34	-13.88	-16.06											
	0.82	-35.35	-28.98	-15.29	-13.66	-10.29	-19.24	-14.66	-14.66											
	0.77	-17.29	-28.47	-12.91	-10.54	-12.33	-16.75	-12.89	-13.29	-13.38										
	0.73	-10.77	-30.84	-8.78	-3.88	-12.84	-17.23	-10.98	-13.31	-10.77										
	0.68	-19.45	-29.61	-12.71	-9.66	-12.92	-19.68	-8.70	-12.38	-12.05	-12.91									
	0.64	-15.86	-30.59	-18.92	-17.67	-14.06	-18.60	-9.52	-13.06	-10.91	-9.61	-8.02								
	0.59	-21.91	-28.38	-18.50	-17.93	-15.70	-21.56	-10.25	-13.85	-12.18	-8.24	-9.76	-9.17							
	0.55	-32.02	-29.66	-23.10	-23.66	-11.84	-19.75	-9.71	-14.11	-13.84	-9.44	-9.30	-7.57	2.23						
	0.50	-31.40	-29.83	-26.28	-27.89	-14.72	-23.70	-8.40	-15.29	-12.91	-8.33	-5.50	-7.10	3.90	-0.36					
	0.45	-28.83	-30.65	-24.59	-25.17	-14.79	-24.06	-9.50	-15.43	-12.85	-5.77	-6.60	-6.73	5.25	-3.55					
	0.41	-29.69	-37.17	-29.28	-28.83	-16.69	-26.87	-8.80	-16.02	-12.06	-7.30	-9.34	-7.00	2.42	-3.55					
	0.36	-14.76	-40.42	-28.88	-26.85	-14.59	-24.85	-7.40	-13.32	-10.12	-6.49	-7.76	-4.75	2.42	-0.70					
	0.32	-36.14	-39.27	-33.10	-33.09	-16.74	-25.92	-9.42	-11.28	-10.24	-5.96	-5.84	-2.19	3.03	-6.20					
	0.27	-38.44	-40.92	-31.13	-29.57	-16.75	-26.45	-7.86	-6.34	-10.32	-3.63	-4.36	-1.11	5.36	-5.14					
	0.23	-23.77	-43.19	-35.79	-34.99	-17.91	-25.52	-5.13	-3.28	-11.11	-3.90	-3.04	0.44	5.51	0.37					
	0.18	-41.14	-42.17	-36.04	-35.69	-19.03	-31.01	-6.26	-1.23	-13.50	-4.22	-3.04	0.48	3.53	1.98					
	0.14	-33.13	-40.07	-36.73	-37.48	-20.03	-34.16	-5.77	-5.28	-11.49	-6.81	-0.58	-1.67	5.48	2.08					
0.09	-32.46	-43.54	-38.84	-38.88	-22.04	-37.71	-6.09	-10.59	-14.11	-11.62	-2.29	-3.25	2.34	2.63						
0.05	-28.61	-47.63	-41.36	-40.58	-24.16	-39.36	-7.73	-12.37	-12.22	-11.46	-10.02	-8.19	2.04	1.73						
0.00	-65.52	-60.58	-54.65	-53.58	-50.63	-50.56	-47.38	-47.51	-45.03	-44.96	-41.08	-35.56	-25.59	-24.93						

is obtained in the low torque and speed region, where errors of around 35 to 40 % can be encountered. The bigger estimation errors are once again related to the no-load torque value.

For this model, in contrast to the baseline, estimation performance is not perfectly consistent across the operating conditions, showing significant improvement at higher rotational speeds (i.e. above the base speed) and at high torque values in the lower rpm region.

4.1.3 Performance Comparison of the Models on the First Motor

To compare the performance of the two estimations, Table 4.3 reports the difference in absolute percentage error of the baseline model and the variable coefficient model. Cells highlighted in green refer to better accuracy for the VarKhKc model whereas red cells indicate worse accuracy for the VarKhKc model. This representation allows graphical visualization of the region of the torque-speed range where implementing the more complicated estimation method would yield a significant benefit. Higher prediction accuracy happens in the higher half of the rpm range, with an increase of more than 30% in certain operating conditions.

4.1.4 Mean Absolute Percentage Error and Speed Range Subdivision Analysis on the First Motor

The best way to assess the overall estimation performance of the models across all the operating conditions is the mean absolute percentage error, which is reported in

Table 4.4 for different ranges of operating conditions. When considering the entire speed and torque range, the newly implemented estimation method shows an improvement of almost 20%, reducing the MAPE from 36.80% of the baseline model down to 17.70%.

As noted before, the VarKhKc model is better performing at higher speeds. This is clearly shown by the MAPE figure when solely considering the region above the base speed (i.e. from 7000 to 14000 rpm). In this region the improvement achieved is of over 27%, reducing the error of 37.38% of the default estimation method to an error lower than 10% of the VarKhKc model.

The same performance evaluation was repeated removing from the calculation the bad-performing no-load torque value, but without a noticeable difference. When limiting the torque range as described, the VarKhKc model performs even better above the base speed, with a MAPE of only 7.87 %.

4.2 Performance Analysis on the Second Motor

In this section the percentage difference of each estimation with respect to the test data will be presented and analyzed, together with a comparison of the prediction errors of the two estimation methods. Furthermore, the data will be analyzed focusing on two different speed ranges to highlight the estimation behavior of the newly implemented method.

4.2.1 Baseline Model Performance Analysis on the Second Motor

The percentage error of the baseline model, reported in Table 4.5, shows a significant underestimation of the loss across all the operating conditions. The percentage error reaches critical values, above 60%, in the higher rpm region whereas the model shows better accuracy, although always quite poor, in the lower rpm region, with errors ranging mostly between 30% and 45%.

Table 4.3. Absolute percentage error difference between VarKhKc and baseline models

Absolute Percentage Error Difference		Speed [rpm]																		
		1000	2000	3000	4000	5000	6000	7000	8000	9000	10000	11000	12000	13000	14000					
Torque/Max Torque	1.00	14.50	22.69	23.20	31.50	20.69	20.63													
	0.95	2.77	19.92	24.51	28.58	21.82	20.22	27.40												
	0.91	-4.47	13.44	18.92	24.22	22.15	20.33	27.98												
	0.86	7.23	11.48	9.13	18.45	22.93	20.26	27.61	26.69											
	0.82	-4.56	5.21	8.16	18.73	24.75	20.26	26.41	27.28											
	0.77	11.06	5.44	-3.44	20.98	24.32	21.86	27.40	28.02	27.89										
	0.73	15.54	3.72	7.11	28.42	24.06	21.11	28.19	27.93	29.34										
	0.68	6.19	3.91	12.28	26.62	24.46	19.62	29.62	28.41	28.47	29.27									
	0.64	11.56	3.61	5.96	18.25	22.87	20.17	28.66	27.75	28.93	30.36	31.82								
	0.59	6.09	5.23	10.34	18.06	21.78	18.14	28.09	26.98	27.92	30.84	30.15	30.30							
	0.55	-1.74	3.20	10.15	13.80	25.25	19.21	28.32	26.32	26.65	29.80	29.95	30.67	36.75						
	0.50	-1.03	4.60	10.28	10.82	23.07	16.54	29.30	25.20	26.98	29.68	31.94	30.67	33.92	37.23					
	0.45	0.40	3.79	8.89	13.33	22.86	16.37	28.77	24.68	26.17	31.01	30.18	30.48	31.44	33.51					
	0.41	1.81	0.73	7.45	10.70	22.68	14.62	29.86	24.25	26.26	29.49	28.13	30.01	35.20	33.52					
	0.36	14.34	-1.81	6.75	12.19	23.20	15.63	30.25	25.56	27.01	29.24	27.94	30.56	33.81	34.31					
	0.32	-4.24	-2.19	4.25	6.87	21.62	14.61	28.05	26.40	26.27	28.75	28.39	31.07	31.65	26.76					
	0.27	-5.11	-3.38	6.96	9.21	20.87	13.31	28.47	29.10	25.80	29.70	28.37	30.49	26.99	25.10					
	0.23	4.11	-4.97	3.15	4.49	19.13	13.32	30.03	30.57	24.84	29.17	28.39	30.33	25.58	28.12					
	0.18	-7.30	-3.01	3.48	4.51	18.95	9.75	29.29	31.75	23.56	29.65	28.35	29.53	27.36	24.49					
	0.14	-1.14	-1.18	5.81	3.99	18.89	7.76	29.59	29.12	25.21	27.59	30.22	29.66	24.53	23.76					
0.09	1.55	-1.41	5.47	4.39	18.45	6.96	30.90	26.44	24.56	26.12	30.48	29.35	30.05	23.40						
0.05	6.72	-0.65	8.31	6.38	19.20	8.57	31.60	27.51	27.83	27.25	26.89	27.58	31.69	26.37						
0.00	-9.82	-5.07	0.61	1.40	4.06	3.86	6.77	6.37	8.64	8.42	9.12	10.44	16.96	15.38						

Table 4.4. MAPE comparison of baseline and VarKhKc models

Model	Speed range	Torque range	MAPE
Baseline	Full	Full	36.80 %
VarKhKc	Full	Full	17.70 %
Improvement	Full	Full	19.10 %
Baseline	Above base speed	Full	37.38 %
VarKhKc	Above base speed	Full	9.79 %
Improvement	Above base speed	Full	27.59 %
Baseline	Full	No-load excluded	35.97 %
VarKhKc	Full	No-load excluded	16.12 %
Improvement	Full	No-load excluded	19.85 %
Baseline	Above base speed	No-load excluded	36.60 %
VarKhKc	Above base speed	No-load excluded	7.87 %
Improvement	Above base speed	No-load excluded	28.73 %

4.2.2 Variable Coefficients Model Performance Analysis on the Second Motor

The percentage error of the VarKhKc model estimate with respect to the test data is reported in Table 4.6. The estimation is lower than the measured value across all operating conditions, with quite consistent errors in the order of 25% to 40%. From this table it's possible to further address the data points highlighted by Table 3.6 and previously mentioned in section 3.3.3; it shows that the model is both overestimating the loss at 1600 rpm and underestimating it at 2400 and 3200 rpm, when comparing the results to the rest of the operating conditions.

The highest accuracy is obtained in the top rpm region, above 7000 rpm, where the errors are mostly between 20% and 35%.

4.2.3 Performance Comparison of the Models on the Second Motor

The performance comparison of the two models is carried out by looking at the difference between the absolute percentage errors, which is reported in Table 4.7. When looking at the lower rpm region, this comparison shows an unreasonable improvement at 1600 rpm, which must be discarded due to unreasonable trend in the estimate of the VarKhKc model; the same can be said about the performance decrease registered at 2400 and 3200 rpm.

The two models perform similarly in the mid rotational speeds, between 4000 and 8000 rpm, being within 10% of each other. On the other end, significant improvement is achieved in the upper speed range, with error reduction in the order of 30% and peaks as high as 40%; this can be extremely significant given the high iron loss registered in these operating conditions, as the delta between the two estimations for some of these points exceeds 1 kW.

Table 4.5. Percentage error of the baseline model estimation on the second IPMSM

Percentage error - Baseline model	Speed [rpm]																			
	800	1600	2400	3200	4000	4800	5600	6400	7200	8000	8800	9600	10400	11200	12000	12800	13600	14400	15200	16000
1.00	-50.62	-44.97	-38.57	-38.48	-28.02															
0.95	-49.77	-45.14	-37.71	-37.98	-26.97	-31.18														
0.90	-49.02	-44.05	-37.54	-37.65	-25.37	-30.76														
0.85	-48.46	-43.93	-37.29	-37.35	-24.95	-30.74														
0.80	-48.96	-42.77	-36.31	-36.51	-24.04	-28.60	-38.84													
0.76	-49.35	-43.04	-36.21	-36.57	-23.79	-27.14	-37.71													
0.71	-47.56	-43.08	-35.90	-36.49	-23.37	-25.62	-37.05	-43.94												
0.66	-47.54	-42.31	-34.99	-35.19	-21.91	-23.15	-34.90	-44.28												
0.61	-48.49	-42.87	-36.34	-35.78	-22.15	-21.71	-32.97	-43.58	-50.66											
0.56	-47.32	-41.87	-35.13	-36.28	-22.30	-20.20	-31.30	-42.35	-48.28	-57.91										
0.51	-45.49	-40.74	-33.60	-36.60	-21.36	-18.66	-30.16	-39.58	-48.62	-54.09										
0.46	-44.81	-39.63	-32.37	-34.83	-20.79	-17.74	-27.80	-39.30	-46.68	-52.69	-55.08									
0.41	-44.84	-39.66	-32.14	-34.98	-22.55	-17.54	-26.36	-36.26	-44.26	-51.42	-53.50	-56.88								
0.37	-43.94	-41.07	-33.19	-33.30	-20.32	-16.56	-24.53	-37.10	-44.13	-50.83	-54.31	-55.56	-56.47	-58.13						
0.32	-47.56	-44.11	-35.04	-35.75	-23.86	-19.22	-24.19	-36.76	-44.99	-50.63	-54.90	-56.83	-55.08	-55.71	-58.88	-60.93				
0.27	-46.68	-42.29	-36.30	-37.80	-25.54	-21.33	-24.96	-36.02	-45.17	-51.89	-55.54	-58.39	-56.72	-58.38	-58.06	-58.91	-57.96	-61.11		
0.22	-46.53	-44.34	-38.50	-38.75	-28.15	-23.70	-26.88	-35.14	-45.28	-52.30	-55.54	-59.16	-59.84	-60.00	-60.74	-59.75	-61.22	-60.48	-59.60	-61.43
0.17	-49.67	-48.82	-42.03	-44.30	-27.20	-23.49	-28.29	-33.93	-44.11	-51.93	-57.08	-59.91	-61.07	-61.69	-62.45	-61.55	-63.66	-63.43	-62.83	-63.49
0.12	-51.55	-51.43	-46.91	-44.70	-30.99	-29.18	-28.96	-33.25	-43.97	-51.96	-56.56	-61.25	-61.32	-62.73	-64.07	-63.19	-64.93	-65.45	-64.53	-64.76
0.07	-56.09	-47.85	-47.85	-47.90	-38.54	-36.30	-35.67	-36.33	-43.00	-50.88	-57.25	-60.40	-62.23	-64.33	-65.27	-64.28	-66.41	-66.70	-66.37	-66.73
0.02	-56.63	-59.22	-50.34	-50.21	-41.58	-39.89	-38.56	-39.20	-40.32	-49.03	-56.98	-60.61	-62.78	-64.72	-65.86	-65.48	-67.25	-67.91	-67.54	-68.07
0.00	-63.26	-58.04	-52.89	-52.35	-44.43	-45.07	-45.42	-45.45	-45.15	-44.57	-43.85	-42.90	-41.64	-40.28	-39.37	-39.92	-40.34	-39.89	-39.09	-40.03

09

Table 4.6. Percentage error of the VarKhKc model estimation on the second IPMSM

Percentage error - VarKhKc model	Speed [rpm]																			
	800	1600	2400	3200	4000	4800	5600	6400	7200	8000	8800	9600	10400	11200	12000	12800	13600	14400	15200	16000
1.00	-30.98	-8.33	-60.90	-56.49	-45.06															
0.95	-29.53	-2.39	-60.24	-55.89	-44.03	-42.03														
0.90	-29.17	-8.52	-60.01	-55.14	-42.48	-40.67														
0.85	-33.74	-3.64	-59.27	-54.59	-41.56	-39.95														
0.80	-35.65	2.05	-58.04	-53.64	-40.72	-38.91	-36.68													
0.76	-33.82	2.51	-57.82	-53.52	-40.18	-37.80	-34.56													
0.71	-35.48	-8.52	-57.25	-53.05	-39.47	-36.45	-32.47	-33.95												
0.66	-27.55	0.57	-56.29	-51.76	-38.14	-34.59	-32.29	-33.70												
0.61	-31.43	6.37	-56.78	-51.79	-37.86	-33.26	-32.97	-35.19	-39.67											
0.56	-29.54	-10.24	-55.88	-52.28	-37.79	-31.98	-33.72	-37.05	-37.68	-49.15										
0.51	-29.72	14.18	-54.81	-52.28	-36.97	-30.79	-30.82	-33.00	-40.58	-43.94										
0.46	-30.76	-2.42	-53.80	-50.88	-36.36	-29.79	-32.67	-36.74	-40.34	-44.27	-38.44									
0.41	-27.98	-2.05	-53.42	-50.96	-37.42	-29.77	-27.75	-28.68	-38.21	-41.18	-35.51	-42.91								
0.37	-26.20	4.12	-53.73	-49.51	-35.70	-29.02	-33.29	-38.48	-39.40	-38.01	-35.66	-39.90	-36.97	-36.58						
0.32	-28.47	-13.31	-54.88	-51.35	-37.89	-30.80	-34.13	-38.65	-39.73	-35.50	-35.27	-40.94	-35.64	-31.91	-33.70	-15.74				
0.27	-26.78	-9.88	-55.35	-52.91	-39.70	-32.59	-34.42	-37.77	-42.05	-36.70	-34.31	-44.88	-36.62	-33.68	-31.95	-10.59	-17.95	-27.67		
0.22	-25.45	-7.50	-57.48	-54.34	-42.26	-35.14	-34.13	-35.09	-42.45	-41.73	-33.72	-44.78	-37.48	-33.67	-33.63	-17.11	-20.64	-25.43	-20.99	-24.33
0.17	-23.90	-20.91	-62.27	-59.76	-42.57	-35.92	-34.66	-34.78	-40.97	-45.18	-36.92	-46.87	-36.19	-33.42	-35.07	-18.14	-23.69	-29.81	-29.65	-27.64
0.12	-29.20	-29.98	-65.36	-61.52	-48.35	-43.53	-38.37	-35.10	-42.03	-47.06	-36.09	-48.76	-32.37	-32.72	-36.66	-21.35	-25.43	-32.62	-33.60	-32.41
0.07	-38.49	-26.53	-66.47	-64.80	-55.12	-50.88	-42.92	-37.50	-37.67	-38.86	-32.59	-38.98	-34.22	-31.98	-36.13	-24.52	-27.84	-34.71	-37.77	-34.33
0.02	-36.27	-30.88	-67.98	-66.19	-57.52	-52.39	-45.49	-40.82	-30.08	-32.64	-29.84	-38.92	-33.40	-27.93	-33.46	-25.18	-28.50	-35.18	-37.64	-34.73
0.00	-47.88	-34.59	-71.40	-66.45	-58.48	-56.72	-54.62	-53.29	-50.99	-48.42	-45.03	-41.50	-37.97	-34.86	-32.64	-31.47	-29.90	-29.19	-28.82	-26.51

Table 4.7. Absolute percentage error difference between VarKhKc and baseline models on the second IPMSM

Absolute Percentage Error Difference	Speed [rpm]																			
	800	1600	2400	3200	4000	4800	5600	6400	7200	8000	8800	9600	10400	11200	12000	12800	13600	14400	15200	16000
1.00	19.64	36.64	-22.34	-18.01	-17.04															
0.95	20.24	42.75	-22.53	-17.91	-17.06	-10.84														
0.90	19.86	35.53	-22.46	-17.49	-17.11	-9.91														
0.85	14.72	40.29	-21.98	-17.23	-16.61	-9.22														
0.80	13.30	40.71	-21.74	-17.13	-16.68	-10.31	2.16													
0.76	15.53	40.53	-21.61	-16.94	-16.39	-10.66	3.15													
0.71	12.08	34.55	-21.35	-16.56	-16.10	-10.84	4.58	9.99												
0.66	19.99	41.75	-21.30	-16.57	-16.23	-11.44	2.62	10.59												
0.61	17.06	36.50	-20.44	-16.02	-15.71	-11.55	0.00	8.38	11.00											
0.56	17.78	31.63	-20.75	-16.00	-15.50	-11.78	-2.42	5.30	10.61	8.77										
0.51	15.77	26.55	-21.21	-15.68	-15.61	-12.13	-0.66	6.57	8.04	10.15										
0.46	14.06	37.21	-21.43	-16.04	-15.57	-12.04	-4.87	2.56	6.34	8.42	16.64									
0.41	16.85	37.61	-21.28	-15.98	-14.87	-12.23	-1.39	7.58	6.05	10.24	17.99	13.97								
0.37	17.74	36.95	-20.54	-16.21	-15.38	-12.45	-8.76	-1.38	4.73	12.82	18.66	15.66	19.50	21.55						
0.32	19.09	30.80	-19.85	-15.60	-14.03	-11.58	-9.94	-1.88	5.26	15.13	19.63	15.88	19.43	23.80	25.18	45.19				
0.27	19.90	32.41	-19.06	-15.12	-14.16	-11.26	-9.46	-1.75	3.12	15.18	21.23	13.51	20.11	24.69	26.11	48.32	40.01	33.44		
0.22	21.08	36.84	-18.98	-15.59	-14.11	-11.44	-7.25	0.05	2.82	10.57	21.82	14.38	22.36	26.33	27.10	42.64	40.58	35.05	38.61	37.10
0.17	25.77	27.91	-20.24	-15.46	-15.38	-12.43	-6.37	-0.85	3.14	6.75	20.16	13.04	24.88	28.27	27.38	43.41	39.98	33.62	33.18	35.84
0.12	22.35	21.45	-18.45	-16.81	-17.37	-14.35	-9.41	-1.85	1.94	4.90	20.47	12.49	28.95	30.01	27.41	41.84	39.50	32.83	30.93	32.36
0.07	17.60	21.32	-18.61	-16.90	-16.58	-14.58	-7.26	-1.17	5.33	12.02	24.66	21.42	28.01	32.35	29.15	39.75	38.57	31.99	28.60	32.40
0.02	20.36	28.34	-17.64	-15.97	-15.94	-12.51	-6.93	-1.62	10.24	16.39	27.14	21.69	29.38	36.78	32.40	40.30	38.75	32.73	29.90	33.34
0.00	15.38	23.46	-18.50	-14.10	-14.06	-11.66	-9.20	-7.84	-5.84	-3.85	-1.18	1.41	3.66	5.42	6.73	8.44	10.44	10.70	10.27	13.52

4.2.4 High Speed Mean Absolute Percentage Error and Absolute Loss Difference Analysis on the Second Motor

To better appreciate the improvement achieved in the high-speed region, the mean absolute percentage error and average absolute loss of the two estimations will be analyzed and compared in this section. The MAPE of the two models, along with the average iron loss estimate, evaluated in the region above 7000 rpm, is reported in Table 4.8.

The mean absolute percentage error is rather high for both estimation methods, measuring 55.93% when using the default iron loss estimation and 34.61% with the newly implemented method. Although the accuracy obtained using the variable coefficients model may not be considered sufficient yet, the performance improvement with respect to the baseline exceeds 20%, which is a significant achievement. This is reflected in the average iron loss estimation figures: in this speed range, where iron loss is

Table 4.8. MAPE and average iron loss estimate comparison of the two models above 7000 rpm on the second IPMSM

Model	MAPE	Average Iron Loss Estimate
Baseline	55.93 %	793.5 W
VarKhKc	34.61 %	1250.6 W
Improvement	21.31 %	457.1 W

the dominant loss component in the machine, the improvement in iron loss estimate on average is in the order of 500 Watts, which is a substantial amount. The difference (in Watts) between the estimation of loss of the two models is even more apparent at the high-speed region; for example, over 1kW difference is noted at max speed and max torque condition.

4.3 Discussion

4.3.1 Magnetic Induction Analysis

To address the prediction behavior of the variable coefficient model in the specific speed range between 1600 rpm and 3200 rpm, an analysis of the magnetic induction magnitude has been conducted to determine whether the two models were given the same B field distribution by the software. The plots in Figures 4.1a and 4.1b show the magnetic induction magnitude in the stator and the rotor of the machine when using the two iron loss models, at the operating point of 0.51 pu torque and 1600 rpm.

As expected, the magnetic induction plots in the two different cases are identical. This is due to the fact that the difference between the two estimation methods resides in the iron loss model and algorithm, and not in any of the inputs parameters that determine the B field distribution (i.e. the input current). This is confirmed also by a second analysis, carried out at a different rotational speed (2400 rpm); the results are shown in Figures 4.2a and 4.2b.

Having performed this check, the cause of the inconsistency must reside in the iron loss computation algorithm, which is defined by the external control program. Being the source code of the program accessible, a review of the code was done to spot a possible cause of the phenomenon but the effort was unsuccessful, partially due to a lack

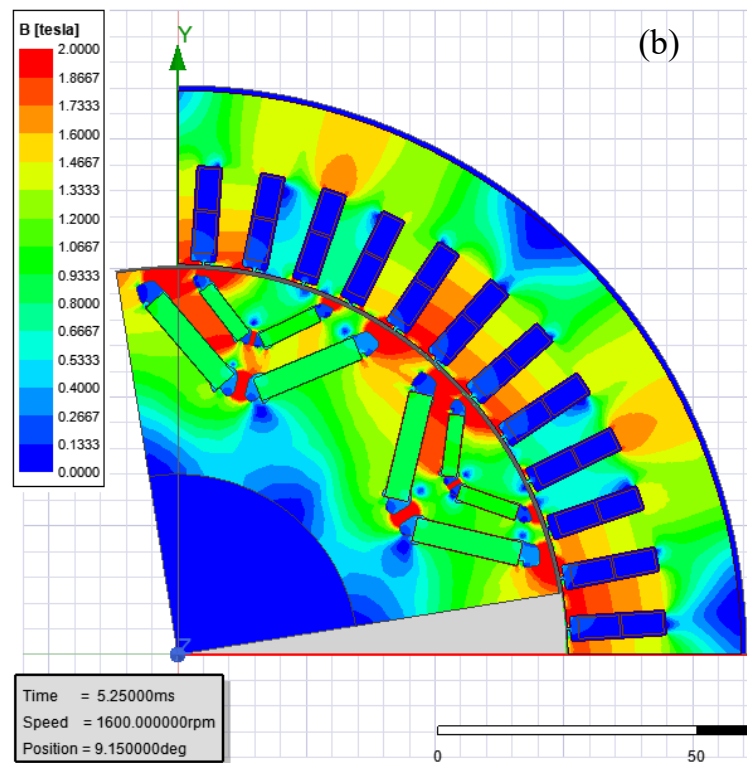
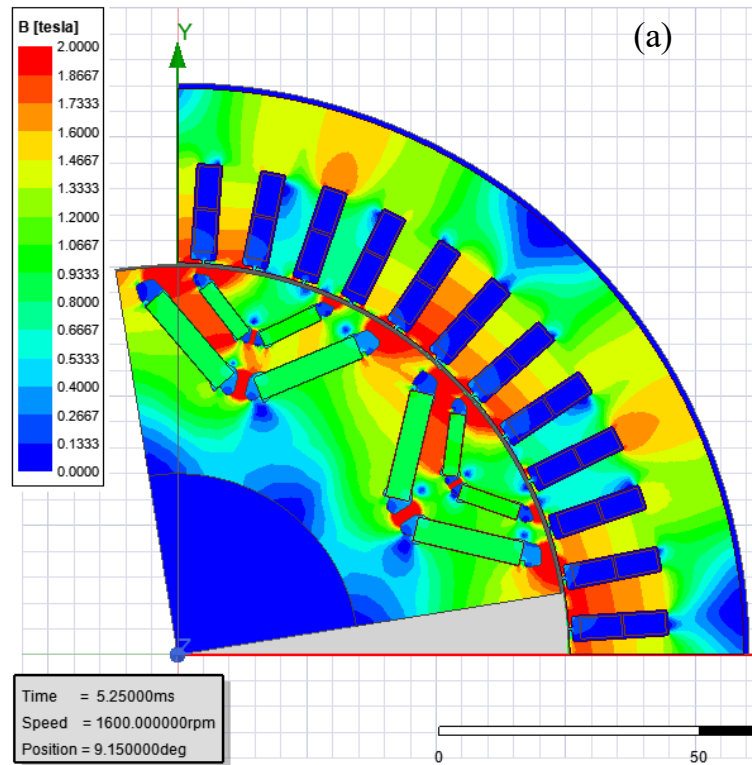


Figure 4.1. Magnetic induction magnitude plot at 1600 rpm and 0.51 pu torque of the default simulation (a) and variable coefficients simulation (b)

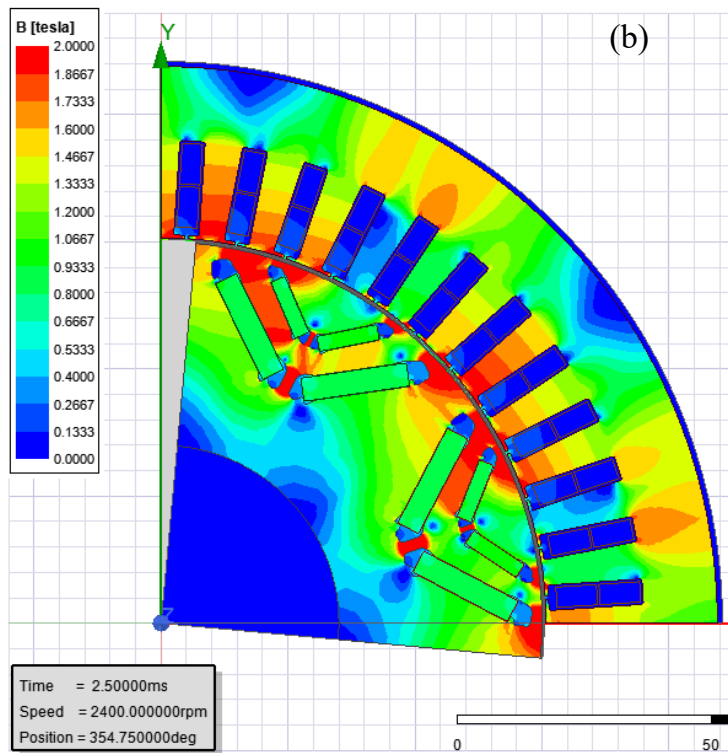
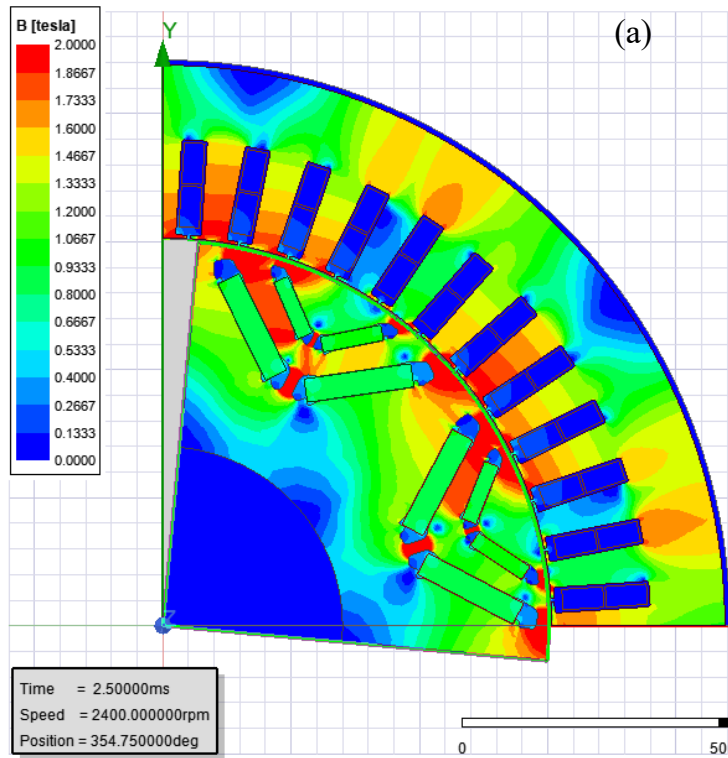


Figure 4.2. Magnetic induction magnitude plot at 2400 rpm and 0.51 pu torque of the default simulation (a) and variable coefficients simulation (b)

of advanced coding knowledge of the author. Being able to find a potential point of improvement of the code can be considered an accomplishment of this research, opening up to the necessity of a more in-depth review on Ansys side to address it. The out of trend data is easy to spot when assessing the results and very limited in the operating conditions in which it appeared (in fact this phenomenon didn't happen in any working point when analyzing the first motor).

4.3.2 Estimation Accuracy Comparison Between Motors

Implementing the developed iron loss estimation method on another electric motor allowed for better insight on the behavior of the iron loss model when applied to a different environment; the points of similarity and contrast of the two applications are going to be highlighted and analyzed in this section.

When looking at the estimation accuracy of the variable coefficients model on the two motors, reported respectively in Tables 4.2 and 4.6, it is clear that the model performs better on the first motor, yielding a more accurate estimate across all operating conditions. This does not happen exclusively on the newly implemented iron loss estimation method, as the same estimation accuracy discrepancy is mostly reflected also in the default model results, reported for the two motors in Tables 4.1 and 4.5, respectively.

Many factors differentiate the two motors and two datasets are not enough to build a definite correlation. Saturation level in the magnetic core of the two machines has been analyzed at the maximum achievable torque at the base speed, respectively 6000 rpm and 4600 rpm, and the highest achievable torque at the maximum rotational speed, respectively 0.5 pu torque at 14000 rpm and 0.22 pu torque at 16000 rpm. The magnetic induction magnitude is plotted for each of the aforementioned conditions in

Figures 4.3, 4.4, 4.5 and 4.6; the maximum reported magnetic induction value on the scale is $B=1.8$ T for all the plots.

When looking at the saturation levels in the worst-case scenario, i.e. maximum torque at the base speed of the motor, it is possible to observe that motor 1 manifests a slightly higher saturation level in the stator teeth whereas a high saturation level is present in the rotor of motor 2, due to the different magnet configuration.

Similarly, when analyzing the maximum speed working condition, it is still possible to observe higher saturation levels above the magnets in the second motor, whereas both machines reach high B values in the stator only in the tooth tip region, which is to be expected.

Finally, both estimation methods use an iron loss model unable to determine the additional loss due to the presence of minor loops, caused by reversals in the flux density waveform; this phenomenon, as discussed in chapter 1, is emphasized by the presence of PWM current supply. The region most interested by the minor loops is typically above the magnets in the rotor, which could explain the higher average discrepancy between the estimations of both models and the test results in the second motor.

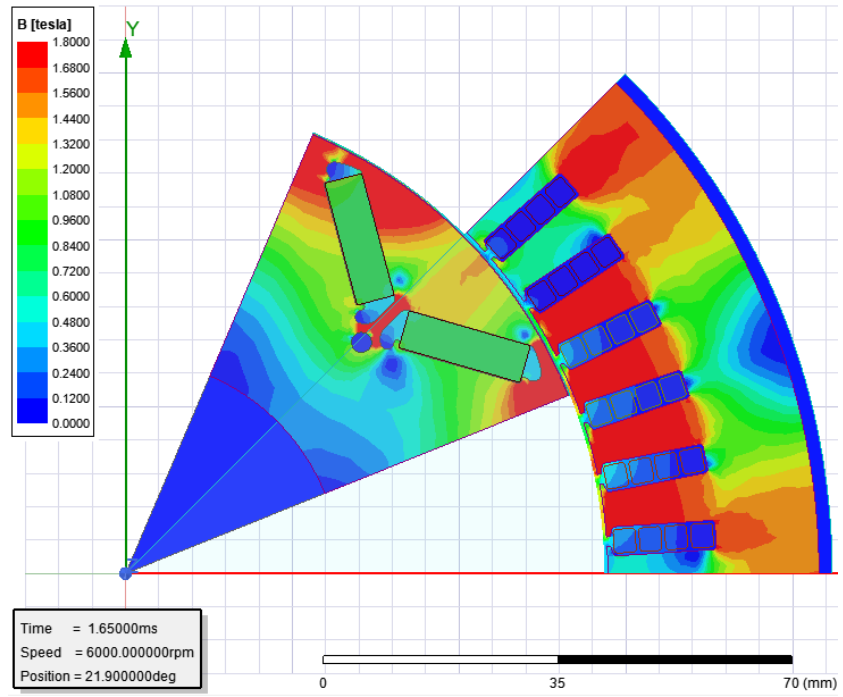


Figure 4.3. Magnetic induction magnitude plot of the first motor at 6000 rpm and 1 pu torque

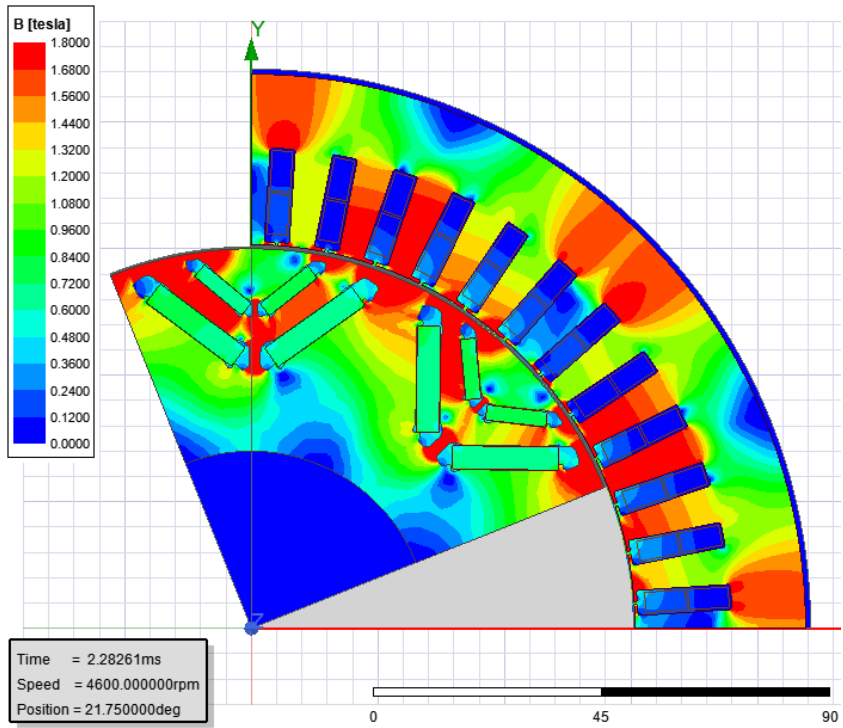


Figure 4.4. Magnetic induction magnitude plot of the second motor at 4600 rpm and 1 pu torque

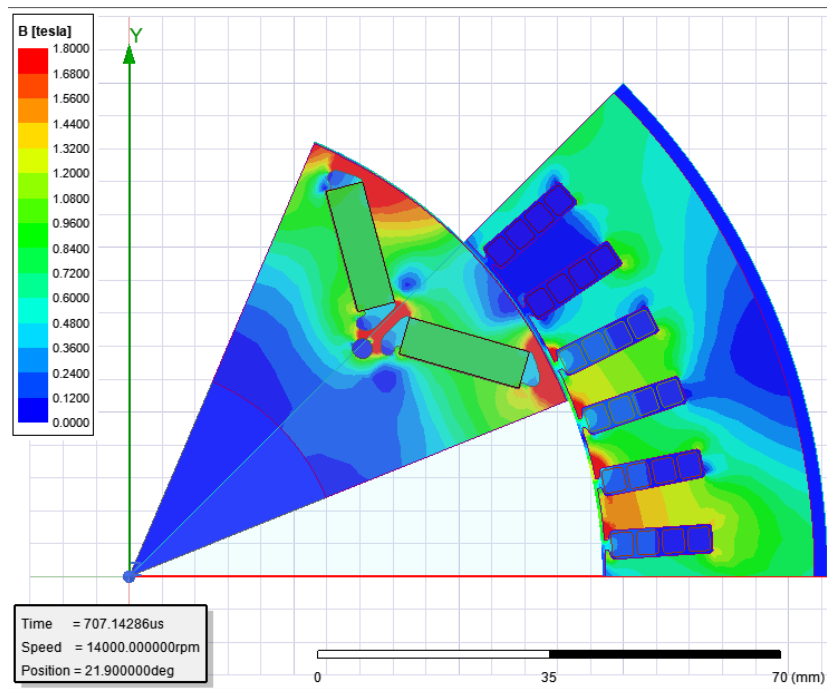


Figure 4.5. Magnetic induction magnitude plot of the first motor at 14000 rpm and 0.5 pu torque

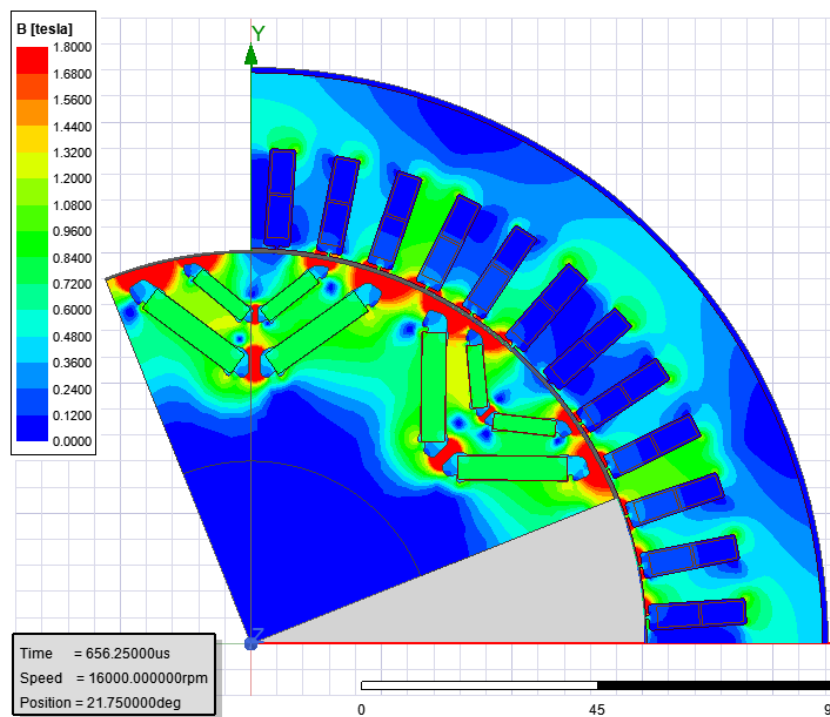


Figure 4.6. Magnetic induction magnitude plot of the second motor at 16000 rpm and 0.22 pu torque

CHAPTER FIVE

CONCLUSIONS AND FUTURE WORK

5.1 Conclusions

In this work the physical origin of iron losses has been studied and presented alongside the influencing factors related to electric motors applications. The concept of iron loss separation has been introduced and the most common modelling techniques related to this approach have been analyzed.

The scope of the research was to accurately estimate iron loss in electric motors used for traction applications. In particular, the work was focused towards interior permanent magnet synchronous motors under pulse width modulation excitation. First, the PWM currents, required as input to the 2D iron loss simulation, were generated using the finite element analysis software Ansys Electronics Desktop. Second, a baseline iron loss estimation was defined using a two-term constant coefficient model in time domain, which is employed as default by the software for the iron loss calculation. A new estimation method, using a variable coefficient frequency domain analysis, has been implemented. The methodology followed has been presented, including the evaluation of the lamination material properties, the acquisition of the variable coefficients, the current generation process and the final implementation in the simulation environment. The default model and variable coefficient model have been applied on two electric machines of different rated power for iron loss estimation.

The comparison of the results between the two estimation methods showed a significant improvement with a mean absolute percentage error reduction close to 20% when considering the entire operating range of the machine, and an even higher

reduction of 27% in flux-weakening conditions. In contrast with the baseline estimation method, the variable coefficient one requires more steps to be implemented and uses an external control program to evaluate the iron loss in post-processing. Given that the current generation procedure is the same and that both simulation methods require the same computational effort, the improvement in prediction accuracy is well worth the trade-off in slightly longer initial setup.

The frequency domain variable coefficient model highlighted an inconsistency in the iron loss estimation in a specific rpm range and only for the second motor. The phenomenon is to be attributed to the code that governs the external control program. The analysis of the results of the second motor showed an overall worse performance of both estimation methods when considering MAPE with respect to the first motor. The benefits of the more articulated simulation procedure are evident again in the flux-weakening operating range, with a MAPE reduction just over 20%.

5.2 Future Work

Though in this work the iron loss estimation method was applied to interior permanent magnet synchronous motors, the same technique could be applied to different electric machine topologies. It would be interesting to apply and validate the model on different motors, such as surface mounted permanent magnet and induction motors.

The prediction accuracy of the presented variable coefficient model justifies its implementation over the default iron loss estimation technique but some code refinement would be beneficial, to reduce or totally eliminate instances of inconsistent model behavior.

Integration of this estimation method on more motors can be the subject of additional research, aimed at creating a correlation between model performance and

motor characteristics, at improving the performance of the model itself and at streamlining its implementation procedure in the finite element analysis software.

APPENDIX A
DATA TABLES

Table A.1. Values of K_h as function of peak magnetic induction

B [T]	K_h
0.1	184.6
0.2	185.4
0.3	170.5
0.4	155.4
0.5	142.9
0.6	132.7
0.7	124.2
0.8	117.5
0.9	112.4
1	108.6
1.1	106.0
1.2	104.9
1.3	105.7
1.4	109.1
1.5	110.7
1.6	106.6
1.7	98.1
1.8	93.6
1.9	88.1

Table A.2. Values of K_c as function of frequency and peak magnetic induction

K_c	f [Hz]				
	50	100	400	1000	2000
B [T]					
0.1	0.48	0.48	0.4	0.37	0.31
0.2	0.49	0.49	0.42	0.35	0.29
0.3	0.49	0.49	0.41	0.33	0.27
0.4	0.48	0.48	0.39	0.31	0.25
0.5	0.47	0.47	0.38	0.3	0.24
0.6	0.45	0.45	0.37	0.29	0.24
0.7	0.44	0.44	0.36	0.28	0.24
0.8	0.43	0.43	0.35	0.28	0.24
0.9	0.42	0.42	0.34	0.28	0.24
1	0.41	0.41	0.34	0.28	0.25
1.1	0.4	0.4	0.34	0.29	0.26
1.2	0.4	0.4	0.34	0.3	0.27
1.3	0.41	0.41	0.34	0.3	0.27
1.4	0.43	0.43	0.36	0.32	0.27
1.5	0.45	0.45	0.38	0.34	0.26
1.6	0.46	0.46	0.39	0.37	0.26
1.7	0.47	0.47	0.41	0.4	0.26
1.8	0.4	0.4	0.42	0.42	0.25
1.9	0.35	0.35	0.43	0.43	0.25

Table A.3. I_d values for PWM current generation

Id [A]	Speed [RPM]													
	1000	2000	3000	4000	5000	6000	7000	8000	9000	10000	11000	12000	13000	14000
1.00	-288.95	-289.00	-289.06	-289.12	-289.18	-289.23								
0.95	-277.90	-277.95	-278.01	-278.06	-278.12	-278.17	-343.87							
0.91	-266.61	-266.66	-266.71	-266.77	-266.82	-266.87	-319.93							
0.86	-244.42	-244.47	-244.52	-244.57	-244.62	-244.67	-295.25	-375.59						
0.82	-233.15	-233.20	-233.25	-233.30	-233.34	-233.39	-271.64	-347.61						
0.77	-219.54	-219.74	-219.94	-220.13	-220.32	-220.51	-247.13	-319.85	-387.47					
0.73	-200.52	-200.57	-200.61	-200.65	-200.69	-200.73	-223.65	-292.72	-355.35					
0.68	-188.70	-188.74	-188.78	-188.82	-188.86	-188.90	-200.11	-266.27	-324.47	-380.52				
0.64	-168.94	-168.98	-169.01	-169.05	-169.08	-169.12	-176.44	-240.23	-294.63	-345.82	-397.63			
0.59	-157.30	-157.33	-157.37	-157.40	-157.44	-157.47	-157.53	-213.93	-265.76	-312.99	-358.82	-405.96		
0.55	-138.27	-138.30	-138.33	-138.36	-138.39	-138.43	-138.46	-188.97	-237.28	-282.08	-322.77	-362.74	-406.55	
0.50	-127.21	-127.24	-127.27	-127.30	-127.33	-127.36	-127.39	-163.29	-209.67	-251.13	-288.81	-324.63	-360.41	-397.67
0.45	-109.47	-109.50	-109.53	-109.55	-109.58	-109.61	-109.63	-137.95	-182.39	-221.35	-256.10	-288.37	-319.92	-350.36
0.41	-96.45	-96.48	-96.50	-96.53	-96.55	-96.57	-96.60	-110.55	-152.14	-187.60	-219.64	-248.61	-275.74	-302.55
0.36	-81.82	-81.85	-81.87	-81.89	-81.91	-81.93	-81.96	-87.58	-127.74	-162.08	-192.70	-220.34	-245.62	-268.96
0.32	-68.19	-68.21	-68.23	-68.25	-68.27	-68.29	-68.31	-68.84	-103.58	-137.07	-166.50	-192.58	-216.64	-238.11
0.27	-59.43	-59.45	-59.47	-59.49	-59.51	-59.53	-59.55	-59.57	-79.94	-112.05	-140.87	-166.19	-188.91	-210.41
0.23	-47.12	-47.14	-47.16	-47.18	-47.19	-47.21	-47.23	-47.25	-55.04	-87.39	-115.67	-140.51	-162.93	-182.97
0.18	-35.79	-35.80	-35.82	-35.83	-35.85	-35.87	-35.88	-35.90	-35.96	-62.43	-90.84	-116.05	-137.72	-158.10
0.14	-24.43	-24.45	-24.47	-24.49	-24.52	-24.54	-24.56	-24.58	-24.60	-38.88	-67.32	-92.11	-115.28	-134.96
0.09	-13.16	-13.18	-13.20	-13.22	-13.24	-13.27	-13.29	-13.31	-13.33	-14.33	-45.08	-71.88	-94.61	-115.73
0.05	-6.22	-6.23	-6.24	-6.25	-6.26	-6.27	-6.28	-6.29	-6.30	-6.31	-27.70	-54.96	-79.90	-101.52

Table A.4. I_q values for PWM current generation

Iq [A]	Speed [RPM]													
	1000	2000	3000	4000	5000	6000	7000	8000	9000	10000	11000	12000	13000	14000
1.00	344.35	344.42	344.49	344.56	344.63	344.69								
0.95	331.18	331.25	331.32	331.38	331.45	331.51	283.24							
0.91	317.73	317.80	317.86	317.92	317.98	318.04	278.98							
0.86	312.64	312.71	312.77	312.83	312.89	312.95	274.35	238.70						
0.82	298.23	298.29	298.35	298.41	298.47	298.53	269.23	233.87						
0.77	285.17	285.11	285.05	284.99	284.93	284.87	263.44	228.32	206.85					
0.73	275.63	275.69	275.75	275.80	275.86	275.92	257.34	222.10	201.40					
0.68	260.24	260.30	260.35	260.41	260.46	260.52	250.10	215.81	195.12	180.93				
0.64	249.95	250.01	250.06	250.12	250.17	250.22	242.82	208.36	188.11	174.25	164.08			
0.59	233.52	233.57	233.62	233.67	233.72	233.77	233.04	200.48	180.43	167.03	157.24	149.46		
0.55	221.43	221.48	221.53	221.58	221.63	221.68	221.73	191.85	172.18	159.15	149.79	142.41	136.32	
0.50	203.73	203.78	203.82	203.87	203.92	203.96	204.01	182.65	163.30	150.47	141.45	134.52	128.99	124.26
0.45	189.61	189.66	189.71	189.75	189.80	189.85	189.89	172.54	153.60	141.17	132.37	125.88	120.71	116.50
0.41	167.06	167.10	167.14	167.19	167.23	167.27	167.31	158.29	140.29	128.25	120.14	113.82	109.17	105.23
0.36	153.77	153.81	153.86	153.90	153.94	153.98	154.02	149.71	131.62	119.97	111.71	105.75	101.09	97.44
0.32	139.59	139.64	139.68	139.72	139.76	139.80	139.84	139.42	122.61	110.83	103.01	96.91	92.51	89.05
0.27	122.15	122.19	122.23	122.27	122.31	122.34	122.38	122.42	112.74	101.41	93.26	87.45	83.36	79.88
0.23	106.02	106.05	106.09	106.13	106.16	106.20	106.24	106.27	102.14	90.52	82.97	77.39	73.00	70.12
0.18	88.66	88.70	88.74	88.77	88.81	88.85	88.89	88.93	88.94	79.39	71.18	65.77	62.27	58.88
0.14	69.31	69.34	69.37	69.41	69.44	69.47	69.51	69.54	69.57	64.65	57.87	53.15	49.22	46.91
0.09	49.25	49.28	49.32	49.35	49.39	49.42	49.45	49.49	49.53	49.12	41.92	37.62	35.42	32.84
0.05	25.02	25.06	25.09	25.13	25.17	25.21	25.25	25.28	25.32	25.37	22.21	20.26	18.51	17.58

Table A.5. I_d values for PWM current generation of the second IPMSM

Id [A]	Speed [rpm]																				
	800	1600	2400	3200	4000	4800	5600	6400	7200	8000	8800	9600	10400	11200	12000	12800	13600	14400	15200	16000	
1.00	-463.44	-462.11	-461.24	-460.63	-482.23																
0.95	-445.06	-450.85	-445.28	-444.80	-460.35	-503.38															
0.90	-414.28	-414.38	-415.65	-415.88	-418.54	-512.84															
0.85	-374.08	-386.46	-384.87	-385.12	-386.32	-486.84															
0.80	-352.07	-350.85	-352.94	-354.24	-352.89	-434.06	-491.37														
0.76	-325.23	-325.04	-324.89	-327.74	-327.46	-390.46	-495.90														
0.71	-299.81	-301.07	-298.00	-302.00	-302.07	-349.65	-457.61	-506.39													
0.66	-272.23	-268.80	-267.23	-266.34	-265.42	-306.18	-398.08	-497.28													
0.61	-249.10	-246.86	-248.90	-243.29	-239.32	-267.67	-347.01	-443.92	-489.08												
0.56	-212.32	-212.87	-217.00	-219.96	-215.26	-233.01	-305.27	-382.38	-471.35	-450.59											
0.51	-176.60	-181.11	-181.88	-196.50	-186.65	-200.45	-262.99	-330.35	-402.60	-432.65											
0.46	-165.06	-169.48	-171.45	-180.17	-178.92	-187.12	-244.29	-307.93	-368.25	-405.72	-448.42										
0.41	-140.40	-145.36	-146.97	-152.35	-159.00	-159.38	-206.57	-262.44	-314.86	-372.63	-428.78	-426.47									
0.37	-121.67	-128.20	-123.29	-120.31	-122.97	-127.97	-168.03	-219.46	-266.32	-312.18	-357.76	-401.16	-425.70	-434.13							
0.32	-112.96	-119.79	-108.12	-104.09	-111.47	-110.66	-134.22	-178.91	-221.09	-259.84	-298.88	-333.02	-376.78	-411.84	-391.32	-406.10					
0.27	-81.61	-76.85	-81.76	-81.66	-86.84	-85.09	-101.61	-139.78	-178.13	-215.49	-247.91	-275.45	-309.21	-338.64	-369.00	-386.04	-408.98	-387.61			
0.22	-59.28	-60.08	-58.21	-57.50	-63.03	-60.13	-75.70	-102.75	-138.27	-172.25	-201.43	-226.15	-251.22	-276.53	-298.64	-318.22	-341.80	-361.13	-376.64	-369.48	
0.17	-43.05	-54.54	-50.82	-49.27	-30.82	-30.05	-48.67	-69.55	-100.56	-131.11	-158.41	-183.16	-205.36	-227.18	-244.98	-262.54	-277.18	-292.63	-309.25	-320.31	
0.12	-26.30	-33.97	-31.18	-23.66	-12.93	-15.86	-18.39	-37.51	-65.83	-94.16	-120.28	-143.99	-165.79	-186.66	-204.27	-218.24	-232.29	-245.07	-256.17	-267.48	
0.07	-12.67	-10.14	-6.51	-7.14	-5.59	-8.40	-7.43	-13.40	-33.80	-61.36	-89.57	-114.36	-136.83	-154.76	-172.57	-186.88	-200.34	-213.71	-222.69	-232.47	
0.02	-5.69	-3.37	-2.85	-3.65	-4.00	-5.37	-5.19	-5.09	-12.01	-42.84	-74.09	-99.01	-120.20	-138.99	-157.92	-172.22	-185.50	-198.76	-206.85	-216.13	

Table A.6. I_q values for PWM current generations of the second IPMSM

Iq [A]	Speed [rpm]																				
	800	1600	2400	3200	4000	4800	5600	6400	7200	8000	8800	9600	10400	11200	12000	12800	13600	14400	15200	16000	
1.00	608.62	609.20	610.69	611.73	580.47																
0.95	585.80	575.71	585.90	586.96	563.21	479.27															
0.90	557.16	557.63	556.01	555.94	551.42	447.55															
0.85	545.15	526.88	529.75	529.01	527.15	422.60															
0.80	506.22	508.06	505.41	503.74	505.53	417.76	355.85														
0.76	479.41	479.64	480.12	476.57	476.86	406.19	337.20														
0.71	454.62	453.27	456.91	452.17	452.14	395.24	323.76	286.67													
0.66	427.46	432.57	434.58	435.67	436.88	388.61	319.72	276.40													
0.61	396.19	399.12	396.32	403.23	408.20	375.86	312.75	269.34	238.53												
0.56	382.77	382.24	377.50	374.27	379.92	359.85	302.56	263.43	233.69	210.49											
0.51	371.13	365.78	365.17	349.37	360.65	344.59	289.11	254.28	229.29	205.85											
0.46	355.93	350.81	348.84	339.65	341.09	331.74	282.98	248.98	225.97	202.42	187.35										
0.41	327.49	322.04	320.26	314.14	308.11	308.91	268.83	236.37	216.12	199.24	183.06	168.32									
0.37	293.02	287.09	291.71	294.15	291.89	287.76	254.01	223.41	203.46	189.15	176.66	164.82	153.57	140.85							
0.32	252.73	246.61	258.07	261.57	255.21	256.12	235.75	206.84	188.65	175.15	164.71	155.80	147.73	139.45	128.97	122.53					
0.27	228.44	231.63	228.18	228.27	225.29	225.96	213.08	189.38	171.95	158.90	149.75	142.47	136.32	130.88	124.99	120.51	112.83	105.62			
0.22	196.62	195.81	196.67	196.81	193.34	195.27	183.58	167.51	151.81	140.63	131.24	125.35	120.28	115.83	111.52	108.45	105.31	102.03	98.37	94.55	
0.17	158.85	150.95	152.46	153.14	164.20	165.51	154.30	143.15	129.06	118.98	110.28	105.21	101.05	97.21	94.03	90.67	88.54	86.49	85.01	83.71	
0.12	118.23	113.09	113.80	117.16	122.41	122.35	121.74	112.88	100.43	92.54	85.04	79.37	76.75	73.86	71.26	69.32	68.01	66.00	64.54	64.77	
0.07	71.24	72.10	73.06	73.16	73.87	73.27	73.50	71.39	64.87	60.30	54.77	50.65	49.38	46.61	45.99	45.06	44.50	42.59	40.66	42.28	
0.02	33.78	35.18	35.39	35.34	35.35	34.82	34.89	35.04	33.46	31.92	30.53	28.41	25.80	25.79	26.90	28.22	28.10	24.97	22.32	23.94	

APPENDIX B
COPYRIGHT PERMISSION LETTERS



A general formula for prediction of iron losses under nonsinusoidal voltage waveform

Author: M. Amar
Publication: Magnetics, IEEE Transactions on
Publisher: IEEE
Date: Sept. 1995

Copyright © 1995, IEEE

Thesis / Dissertation Reuse

The IEEE does not require individuals working on a thesis to obtain a formal reuse license, however, you may print out this statement to be used as a permission grant:

Requirements to be followed when using any portion (e.g., figure, graph, table, or textual material) of an IEEE copyrighted paper in a thesis:

- 1) In the case of textual material (e.g., using short quotes or referring to the work within these papers) users must give full credit to the original source (author, paper, publication) followed by the IEEE copyright line © 2011 IEEE.
- 2) In the case of illustrations or tabular material, we require that the copyright line © [Year of original publication] IEEE appear prominently with each reprinted figure and/or table.
- 3) If a substantial portion of the original paper is to be used, and if you are not the senior author, also obtain the senior author's approval.

Requirements to be followed when using an entire IEEE copyrighted paper in a thesis:

- 1) The following IEEE copyright/ credit notice should be placed prominently in the references: © [year of original publication] IEEE. Reprinted, with permission, from [author names, paper title, IEEE publication title, and month/year of publication]
- 2) Only the accepted version of an IEEE copyrighted paper can be used when posting the paper or your thesis on-line.
- 3) In placing the thesis on the author's university website, please display the following message in a prominent place on the website: In reference to IEEE copyrighted material which is used with permission in this thesis, the IEEE does not endorse any of [university/educational entity's name goes here]'s products or services. Internal or personal use of this material is permitted. If interested in reprinting/republishing IEEE copyrighted material for advertising or promotional purposes or for creating new collective works for resale or redistribution, please go to http://www.ieee.org/publications_standards/publications/rights/rights_link.html to learn how to obtain a License from RightsLink.

If applicable, University Microfilms and/or ProQuest Library, or the Archives of Canada may supply single copies of the dissertation.

BACK

CLOSE WINDOW



An improved estimation of iron losses in rotating electrical machines

Author: G. Bertotti
Publication: Magnetics, IEEE Transactions on
Publisher: IEEE
Date: Nov. 1991

Copyright © 1991, IEEE

Thesis / Dissertation Reuse

The IEEE does not require individuals working on a thesis to obtain a formal reuse license, however, you may print out this statement to be used as a permission grant:

Requirements to be followed when using any portion (e.g., figure, graph, table, or textual material) of an IEEE copyrighted paper in a thesis:

- 1) In the case of textual material (e.g., using short quotes or referring to the work within these papers) users must give full credit to the original source (author, paper, publication) followed by the IEEE copyright line © 2011 IEEE.
- 2) In the case of illustrations or tabular material, we require that the copyright line © [Year of original publication] IEEE appear prominently with each reprinted figure and/or table.
- 3) If a substantial portion of the original paper is to be used, and if you are not the senior author, also obtain the senior author's approval.

Requirements to be followed when using an entire IEEE copyrighted paper in a thesis:

- 1) The following IEEE copyright/ credit notice should be placed prominently in the references: © [year of original publication] IEEE. Reprinted, with permission, from [author names, paper title, IEEE publication title, and month/year of publication]
- 2) Only the accepted version of an IEEE copyrighted paper can be used when posting the paper or your thesis on-line.
- 3) In placing the thesis on the author's university website, please display the following message in a prominent place on the website: In reference to IEEE copyrighted material which is used with permission in this thesis, the IEEE does not endorse any of [university/educational entity's name goes here]'s products or services. Internal or personal use of this material is permitted. If interested in reprinting/republishing IEEE copyrighted material for advertising or promotional purposes or for creating new collective works for resale or redistribution, please go to http://www.ieee.org/publications_standards/publications/rights/rights_link.html to learn how to obtain a License from RightsLink.

If applicable, University Microfilms and/or ProQuest Library, or the Archives of Canada may supply single copies of the dissertation.

BACK

CLOSE WINDOW

07/01/2020

Dear AIP Publishing:

I am completing a Master's thesis at Oakland University entitled "Iron Loss Estimation Under Pulse Width Modulation Excitation in Permanent Magnet Synchronous Motors" I would like your permission to reprint in my thesis excerpts from the following:

Frequency dependence of hysteresis curves in conducting magnetic materials,
D. C. Jiles, Journal of Applied Physics 76, 5849 (1994); doi:
10.1063/1.358399

The excerpts to be reproduced are: Fig. 2: Modeled hysteresis curves of Permalloy 80 at dc, 400, 1000, 3000, and 6000 Hz calculated by incorporating effects of classical eddy current power losses into the hysteresis equation

The requested permission extends to any future revisions and editions of my thesis, including non-exclusive world rights in all languages. These rights will in no way restrict republication of the material in any other form by you or by others authorized by you. Your signing of this letter will also confirm that your company owns the copyright to the above-described material.

If these arrangements meet with your approval, please sign this letter where indicated below. Thank you very much.

Sincerely,

Filippo Bellone

PERMISSION GRANTED FOR THE USE REQUESTED ABOVE:

AIP Publishing

By: S. LoFaso

Title: Manager, Rights and Permissions

Date: 7/9/2020

REFERENCES

- [1] Z. Zhu and D. Howe, “Electrical Machines and Drives for Electric, Hybrid and Fuel Cell Vehicles”, Proceedings of the IEEE, Vol. 95, No. 4, 2007
- [2] K. Chau, C. Chan and C. Liu, “Overview of Permanent-Magnet Brushless Drives for Electric and Hybrid Electric Vehicles”, IEEE Transaction on Industry Electronics, Vol. 55, No. 6, 2008
- [3] E. Barbisio, F. Fiorillo and C. Ragusa, “Predicting Loss in Magnetic Steels Under Arbitrary Induction Waveform and With Minor Hysteresis Loops”, IEEE Transactions on Magnetics, Vol. 40, No. 4, 2004
- [4] M. Ibrahim and P. Pillay, “Core Loss Prediction in Electrical Machine Laminations Considering Skin Effect and Minor Hysteresis Loops”, IEEE Transactions on Industry Applications, Vol. 49, No. 5, 2013
- [5] M. Popescu, D. Ionel, A. Boglietti, A. Cavagnino and M. McGlip, “A General Model for Estimating the Laminated Steel Losses Under PWM Voltage Supply”, IEEE Transactions on Industry Applications, Vol. 46, No. 4, 2010
- [6] V. Ioniță, L. Petrescu, E. Cazacu, E. Pătroi and E. Manta, “Improved Prediction of Hysteresis Losses in Electrical Machine Cores”, The 7th International Conference on Modern Power Systems, 2017
- [7] F. Fiorillo and A. Novikov, “An Improved Approach to Power Loss in Magnetic Laminations under Nonsinusoidal Induction Waveform”, IEEE Transaction on Magnetics, Vol. 26, No. 5, 1990
- [8] M. Amar and R. Kaczmarek, “A General Formula for Prediction of Iron Losses Under Nonsinusoidal Voltage Waveform”, IEEE Transaction on Magnetics, Vol. 31, No. 5, 1995
- [9] Andreas Krings, “Iron Losses in Electrical Machines – Influence of Material Properties, Manufacturing Processes and Inverter Operation”, PhD thesis, KTH School of Electrical Engineering, Stockholm, 2014
- [10] Mehdi T. Kakhki, “Modelling of Losses in a Permanent Magnet Machine Fed by a PWM Supply”, PhD thesis, Université Laval, Québec, 2016
- [11] A. Krings and J. Soulard, “Overview and Comparison of Iron Loss Models for Electrical Machines”, Journal of Electrical Engineering, Vol. 10, No. 3, 2010
- [12] C. Graham, “Physical origin of losses in conducting ferromagnetic materials”, Journal of Applied Physics, Vol. 53, No. 11, 1982

- [13] G. Bertotti, "General Properties of Power Losses in Soft Ferromagnetic Materials", IEEE Transaction on Magnetics, Vol. 24, No. 1, 1988
- [14] G. Bertotti, "Physical interpretation of Eddy Current Losses in Ferromagnetic Materials", Journal of Applied Physics, Vol. 57, No. 6, 1985
- [15] S. Steentjes, G. von Pfingsten, M. Hombitzer and K. Hameyer, "Iron-Loss Model With Consideration of Minor Loops Applied to FE-Simulation of Electrical Machines", IEEE Transactions on Magnetics, Vol. 49, No. 7, 2013
- [16] R. Pei, X. Zhang, L. Zeng and S. Li, "Studies of High-Frequency Iron Core Loss for Synchronous Electric Machines Used in Electric Vehicles", 20th International Conference on Electrical Machines and Systems, 2017
- [17] D. Ionel, M. Popescu, M. McGlip, T. Miller, S. Dellinger and R. Heideman, "Computation of Core Losses in Electrical Machines Using Improved Models for Laminated Steel", IEEE Transaction on Industry Applications, Vol. 43, No. 6, 2007
- [18] J. Lavers, P. Biringer and H. Hollitscher, "A Simple Method of Estimating The Minor Loop Hysteresis Loss in Thin Laminations", IEEE Transaction on Magnetics, Vol. 14, No. 5, 1978
- [19] M. Popescu, D. Dorrell and D. Ionel, "A Study of the Engineering Calculations for Iron Losses in 3-phase AC Motor Models", The 33rd Annual Conference of the IEEE Industrial Electronics Society, 2007
- [20] D. C. Jiles, "Frequency Dependence of Hysteresis Curves in Conducting Magnetic Materials", Journal of Applied Physics, 76, 1994
- [21] R.H. Pry and C.P. Bean, "Calculation of the Energy Loss in Magnetic Sheet Materials Using a Domain Model", Journal of Applied Physics, Vol. 29, No. 3, 1958
- [22] H. Jordan, "Die Ferromagnetischen Konstanten für Schwachwechselfelder", Elektr. Nach. Techn., Vol. 1, 1924
- [23] D. Ionel, M. Popescu, S. Dellinger, T. Miller, R. Heideman and M. McGlip, "On the Variation With Flux and Frequency of the Core Loss Coefficients in Electrical Machines", IEEE Transactions on Industry Applications, Vol. 42, No. 3, 2006
- [24] L. Ma, M. Sanada, S. Morimoto and Y. Takeda, "Prediction of Iron Loss in Rotating Machines With Rotational Loss Included", IEEE Transactions on Magnetics, Vol. 39, No. 4, 2003
- [25] G. Bertotti, A. Boglietti, M. Chiampi, D. Chiarabglio, F. Fiorillo and M. Lazzari, "An Improved Estimation of Iron Losses in Rotating Electrical Machines", IEEE Transactions on Magnetics, Vol. 27, No. 6, 1991

- [26] S. Jacobs, D. Hectors, F. Henrotte, M. Hafner, M. H. Gracia, K. Hameyer and P. Goes, “Magnetic Material Optimization for Hybrid Vehicle PMSM Drives”, *World Electric Vehicle Journal*, Vol. 3, 2009
- [27] S. Xue, J. Feng, S. Guo, J. Peng, W. Chu and Z. Zhu, “A New Iron Loss Model for Temperature Dependencies of Hysteresis and Eddy Current Loss in Electrical Machines”, *IEEE Transaction on Magnetics*, Vol. 54, No. 1, 2018